

# IDENTIFICATION OF TOOL BREAKAGE IN A DRILLING PROCESS

A Thesis Submitted to the College of

Graduate Studies and Research

In Partial Fulfillment of the Requirements

For the Degree of Master of Science

In the Department of Mechanical Engineering

University of Saskatchewan

Saskatoon

By

Ethan James McKibben

## **PERMISSION TO USE**

In presenting this thesis in partial fulfilment of the requirements for a Postgraduate degree from the University of Saskatchewan, I agree that the Libraries of this University may make it freely available for inspection. I further agree that permission for copying of this thesis in any manner, in whole or in part, for scholarly purposes may be granted by the professor or professors who supervised my thesis work or, in their absence, by the Head of the Department or the Dean of the College in which my thesis work was done. It is understood that any copying or publication or use of this thesis or parts thereof for financial gain shall not be allowed without my written permission. It is also understood that due recognition shall be given to me and to the University of Saskatchewan in any scholarly use which may be made of any material in my thesis.

Requests for permission to copy or to make other use of material in this thesis in whole or part should be addressed to:

Head of the Department of Mechanical Engineering

University of Saskatchewan

57 Campus Drive, Room 3B48.4

Saskatoon, Saskatchewan, Canada, S7N 5A9

## ABSTRACT

In an effort to increase machining efficiency and minimize costs, research into tool condition monitoring (TCM) systems has focused on developing methods to allow for unmanned machining. For drilling processes, such systems typically use indirect approaches to monitoring the tool condition by measuring spindle torque and feed force as well as vibrations including acoustic emission (AE – mechanical vibrations faster than 100 kHz). This project aimed to advance the state-of-the-art in the area of TCM by developing a method to detect sudden tool failures in large diameter ( $> 25$  mm) indexable insert drills. This project was a continuation of the research conducted by Mr. R. Griffin (a former MSc student), who developed a model capable of predicting long term wear trends in indexable insert drills [1]. Notably, his model was unable to react to sudden tool breakage due to tool chipping, which was addressed by this project as presented in this thesis.

In order to develop and train models able to detect sudden tool failure, an experiment was developed and installed in the field of the industry partner of this project. The experiment's main feature was a pair of AE sensors added to the existing torque and force sensors. On this setup, experiments were conducted by drilling 2251 holes in workpieces using indexable insert drills with or without the insert breaking. When drilling holes without the insert breaking, the holes were named as *good* ones; and when drilling holes with the insert breaking they were named as *bad* holes. During the drilling process, data was collected from current sensors attached to the spindle motor and feed motor as well as from an AE sensor on the spindle and on the workpiece.

From the signals from the spindle motor current and feed motor current sensors, algorithms were developed to identify and divide the signals of drilling a hole into different sections of the drilling cycle (i.e. entrance, steady-state, exit, etc.). Steady-state time-domain features were extracted from the sensor signals measured for all holes drilled in the experiments and the extracted features were used to train and test the classifier models. These models were cross validated to determine which type of model was the best fit for the drilling data collected. The results from the classifier models show that most of the classifiers tested have the ability to identify sudden tool breakage based on the data recorded in the present study, with varying degrees of success. The naïve Bayes classifier was able to detect the most failures but suffered

from a large number of falsely detected failures. Both the classification tree and linear discriminant analysis classifiers had lower failure detection rates than the naïve Bayes classifier, but did not suffer from the same amount of false positives; as such, these two classifiers had higher overall classification rates than the naïve Bayes.

These results suggest that classification tree and linear discriminant analysis methods are better suited for the drilling application and that the time-domain features should be complemented by others, such as the features extracted from the frequency domain, to accurately diagnose the tool condition. Future research should focus on extracting frequency and time-frequency domain features as these features might contain more information on tool condition. In addition, methods of examining features at the entrance and exit of the holes should be investigated as these two points in the drilling cycle are the most prone to sudden tool failure

## ACKNOWLEDGMENTS

I would like to thank everyone who assisted me with this research project.

I'd like to express my appreciation to my supervisor, Professor Daniel Chen, for his encouragement and support throughout the project. His constructive suggestions as well as the financial support from his research funds are very much appreciated. I also wish to acknowledge the financial support provided by the Department of Mechanical Engineering at the University of Saskatchewan.

My grateful thanks are extended to Ryan Griffin for his patience in teaching me about the experimental equipment and showing me the applications of this research. Also, thanks to Dr. Yu Cao for his assistance in data collection and his insights on data analysis.

I would also like to thank Mitsubishi Hitachi Power Systems Canada Ltd. for their both their financial support and the use of their facility for data collection. I'd specifically like to thank Kyle Georget for his help in machine scheduling and parts acquisition, Andrew Hildebrandt for his help writing the CNC code use for the experiment, and Kris Boychuk and all the shop floor staff who assisted me with this project.

# TABLE OF CONTENTS

PERMISSION TO USE.....	i
ABSTRACT.....	ii
ACKNOWLEDGMENTS .....	iv
TABLE OF CONTENTS.....	v
LIST OF TABLES .....	ix
LIST OF FIGURES .....	x
LIST OF ABBREVIATIONS.....	xii
1. Introduction.....	1
2. Literature Review.....	2
2.1. Background .....	2
2.2. TCM for Drilling Processes .....	3
2.2.1. Sensors for Drilling.....	4
2.2.2. Feature Extraction for Drilling.....	5
2.2.3. Classification Methods for Drilling .....	6
2.3. Industrial Applications of TCM.....	6
3. Research Objectives.....	7
4. Experiment Design.....	9
4.1. Experiment Parameters .....	9
4.2. Experimental Apparatus.....	10

4.2.1. Machine Setup .....	10
4.2.2. Material .....	13
4.1.3. Tooling .....	14
4.2.4. Sensors and Sensor Placement.....	15
4.2.5. Data Collection .....	18
4.3. Experimental Procedure.....	18
4.3.1 Experimental Setup.....	18
4.3.2. Collecting Testing Data .....	19
4.3.3. Commissioning a Method to Force Failures.....	19
4.3.4. Collecting Training Data.....	21
5. Algorithms Developed and Data Analysis.....	23
5.1. Hole Drilling Cycle.....	23
5.1.1. Algorithm to Identify the Process of Drilling a Hole .....	25
5.1.2. Manual Alignment of Hand Recorded Data .....	28
5.1.3. Hole Division Algorithm .....	28
5.1.4. Time Domain Feature Extraction.....	31
5.1.5. Generate Experiment Object.....	33
5.2. Modification of Algorithms .....	33
5.2.1. Down Sampling and Filtering.....	33
5.2.2. Force Peak Algorithm.....	35

5.2.3. Modified Algorithm to Identify the Essential States .....	35
6. Classifier Development and Validation .....	36
6.1. Classifier Selection .....	36
6.1.1. Zero R Classifier .....	37
6.1.2. Linear Classification Tree.....	38
6.1.3. Naïve Bayes Classifier.....	39
6.1.4. Linear Discriminant Analysis Classifier.....	40
6.1.5. Support Vector Machine and K-Nearest Neighbor Classifiers.....	40
6.2. Classifier Development.....	41
6.2.1. Test Classifier Functionality.....	41
6.2.2. Validate Features .....	42
6.2.3. Cross Validation.....	46
7. Results, Discussion, and Limitations .....	47
7.1. Results and Discussion .....	47
7.2. Limitations .....	55
8. Conclusions and Future Work .....	56
8.1. Conclusions.....	56
8.2. Future Work.....	57
8.2.1. Future work on the data analysis .....	57
8.2.2. Future work on experiments .....	57

8.2.3. Implementation .....	58
References .....	59

## LIST OF TABLES

Table 1: Most common signals measured to infer tool condition.....	5
Table 2: Drilling parameters used for testing .....	10
Table 3: Signal abbreviations.....	12
Table 4: Machine parameters tested for forced natural failures .....	20
Table 5: Definition of states of a drilling cycle .....	23
Table 6: Boolean operators used in the find hole algorithm.....	26
Table 7: Values assigned to each feature .....	32

# LIST OF FIGURES

Figure 1: Block diagram of a typical indirect TCM system .....	3
Figure 2: Indexable insert drill and carbide inserts [29] .....	4
Figure 3: Development of overall project at MHPS .....	7
Figure 4: Schematic of HBM used for testing with built in sensors .....	11
Figure 5: Schematic top view of experimental setup .....	12
Figure 6: Workpiece mounting and hole pattern .....	14
Figure 7: AE sensor mounting locations .....	16
Figure 8: Plot of all AEW features shown before and after moving the AEW sensor .....	17
Figure 9: Comparison of undamaged (left) and damaged (right) drill body end .....	21
Figure 10: Drilling states for a single hole .....	24
Figure 11: Flow chart of the algorithm to identify the proces of drilling a hole .....	27
Figure 12: Flow chart of the algorithm to divide the proces of drilling a hole .....	30
Figure 13: Graphical representation of the Zero R classifier for generated data .....	37
Figure 14: Classification tree generated from artificial data .....	38
Figure 15: Two-dimensional naive Bayes classifier generated from artificial data .....	39
Figure 16: Two-dimensional linear discriminant classifier generated from artificial data .....	40
Figure 17: Results from testing classifiers on artificially generated data .....	41
Figure 18: Pearson correlations between all features tested .....	43
Figure 19: All features plotted for run 05 .....	45

Figure 20: Cross validated classifier results .....	49
Figure 21: Confusion matrix outputs for top three classifiers .....	51
Figure 22: Plot of good and bad holes as feature 21 versus feature 5 .....	53
Figure 23: Plot of good and bad holes as feature 28 versus feature 17 .....	53
Figure 24: Scatter of all features (by number) .....	54

## LIST OF ABBREVIATIONS

NC	Numeric Control
CNC	Computer Numeric Control
TCM	Tool Condition Monitoring
MHPS	Mitsubishi Hitachi Power Systems Canada Ltd.
HSS	High Speed Steel
AE	Acoustic Emission
FFT	Fast-Fourier Transform
PSD	Power Spectrum Density
RMS	Root Mean Square
ANN	Artificial Neural Network
NB	Naïve Bayes
CT	Classification Tree
LDA	Linear Discriminant Analysis
KNN	K-Nearest Neighbor
SVM	Support Vector Machine

# 1. Introduction

The manufacturing industry is constantly looking for new ways to cut costs and increase profits. Since the advent of numeric controlled (NC) machining in the 1940s, the industry has been steadily moving toward fully automated manufacturing including unmanned machining [2]. Modern computer numeric controlled (CNC) machines are able to create complex parts with very little interaction from an operator. However, operators are still required to monitor CNC machines to ensure that they are running properly. One of the key reasons operators are required is to monitor tool health – including wear and chipping.

Development of tool condition monitoring (TCM) systems started in the early 1980s as CNC machines started to become more mainstream in manufacturing facilities [3]. These systems aimed to monitor the state of the machine tool to determine when it needed to be replaced due to excessive wear or failure by other methods such as chipping. An early study showed that mechanical failures of CNC machines, including tool failure and tool change time due to failure, accounted for four times as much downtime as failures due to electrical problems [3]. Since research in the field began in the 1980s, many different TCM systems have been developed for a wide variety of machining processes with varying degrees of success.

Mitsubishi Hitachi Power Systems Canada Ltd. (hereafter MHPS) is in the second phase of a joint project with the University of Saskatchewan developing a TCM system for one of their large diameter indexable drills. Currently, the machine requires an operator present at all time when running. In addition, tools are changed at regular intervals to prevent the use of potentially worn out tools. Phase one of the project conducted by Griffin resulted in the successful development of a model capable of predicting tool wear and hole diameter for the processes of drilling 39 mm diameter holes in a tube-sheet made of duplex stainless steel [1]. Results from this research showed that almost twice as many holes could be drilled by a given tool without drilling any out-of-tolerance holes [1]. As the model developed by Griffin was tuned to detect long term wear, it unable to account for sudden failures like those due to tool chipping [1]. This second phase of the project aimed to develop a system capable of diagnosing sudden tool failure that can be run alongside Griffin's wear model. By running both systems in parallel, MHPS will be able to allow tools to run for their entire useful life reducing operator and tooling costs.

## 2. Literature Review

### 2.1. Background

Tool monitoring systems have long been categorized into two main classes – direct and indirect monitoring systems [4], [5]. The direct monitoring systems require that the tool condition be directly measured off of the tool. These direct systems include visual inspection, optical monitoring methods, and electrical resistance monitoring. Although these methods have a high degree of accuracy, they are primarily used in research and seldom used in industry. This lack of adoption by industry is due to the impracticality of using such systems due to physical constraints of the machine, time constraints, and the use of cutting fluid [6].

Research into TCM focuses almost primarily on indirect monitoring systems. These systems monitor properties that can be easily measured without direct access to the tool. Some properties typically measured in indirect systems include spindle current, torque, feed motor current, feed-force, vibration, and acoustic emission. These properties are then related to the tool condition using a known relationship. Indirect monitoring systems are less accurate than direct monitoring systems as the properties they monitor are typically influenced by more than one machining parameter. Some of these parameters include the type of tool, workpiece material, cutting conditions, and workpiece geometry.

Although many different combinations of sensors, features, and classification algorithms have been successfully implemented in a laboratory setting, no single TCM system has been found superior to others. The machining industry is slowly adopting simple TCM systems to aid with the detection of tool breakage and wear. TCM systems developed in research labs tend to have a higher detection rate but are too complex for use in industry [6]. It is widely accepted that the use of more than one signal yields more accurate results [5], [7]–[9] and some authors even go as far as stating that reliable indirect monitoring is impossible with just one signal feature [6].

In order to reliably diagnose tool condition indirectly a general model which involves sensing, feature extraction, and hole classification (Figure 1) has been widely adopted [3], [5], [6], [8]. Although the general model rarely deviates, the selection of system properties to monitor, features to extract, and methods to classify the features has not found universal acceptance for all

machining operations [5], [6], [8]. Sensors used range from simple spindle and feed motor current sensors [4], [10], [11], to cutting force sensors [11]–[14], to vibration and acoustic emission sensors [15]–[17], to more complex custom vision systems [18]. Features extracted consist of time domain [5], [15], [19]–[21], time-frequency domain (typically wavelet analysis) [22]–[24], and frequency domain features [10], [16]. The classification methods used as also vary from simple rule based models [1], [20] to complex artificial neural networks and other machine learning algorithms [16], [18], [19], [25].

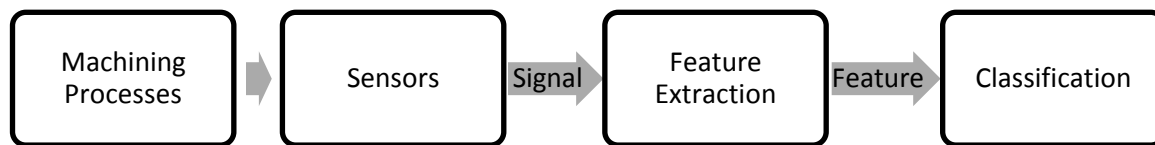


**Figure 1: Block diagram of a typical indirect TCM system**

## **2.2. TCM for Drilling Processes**

Drilling processes have been one of the primary focuses of research into TCM systems [8] and represent about 40% of all cutting operations done in industry [15]. Research into TCM of drilling processes typically focuses on small diameter (< 3 mm diameter) high speed steel (HSS) twist drills [6], [15], [26]–[28] with some research into larger (up to 20 mm diameter) HSS twist drills [19]. Research conducted by Griffin as the first phase of this project was unique as it looked at large diameter holes (> 25 mm) [1]. In addition to using large diameter drills, Griffin also changed the drill geometry. Instead of using the standard HSS twist drill, Griffin used a modern indexable insert drill (Figure 2) – a steel drill body that holds replaceable carbide inserts used for cutting. The following subsections will discuss the sensors (2.2.1.), features (2.2.2.), and classifications methods (2.2.3.) have been studied pertaining to TCM systems for small diameter twist drills. Some studies will also be presented that pertain to mill cutters and turning tools as the carbide coated inserts on these types of tools is similar to those on indexable insert drills.



**Figure 2: Indexable insert drill and carbide inserts [29]**

### **2.2.1. Sensors for Drilling**

A wide variety of sensors have been used to monitor tool condition of drilling processes. The most common sensors are those that monitor the cutting forces [5], [6]. In laboratory settings, these sensors typically involve mounting the workpiece to a dynamometer [11], [12], [14]. While this method results in strong and accurate force signals, it is impractical to apply this monitoring method in industry due to workpiece geometry and size. As such, methods for monitoring the feed force by monitoring the current flowing to the feed motor have been adopted [1], [30]. These methods rely on the relationship between feed motor current and feed motor force to determine the cutting forces. Spindle torque sensors are also commonly used in TCM systems for drilling operations. Similar to cutting force, torque is sometimes measured using rotary torque sensors mounted on the spindle [31] but more commonly measured by monitoring the spindle motor current [5]. Modern drilling and boring machines typically have sensors to monitor motor currents pre-installed for use with TCM systems.

Vibrations have also been monitored in TCM systems for drilling processes [6]. Typical vibration measurements by accelerometers will change significantly under different cutting conditions and work piece properties and are susceptible to environmental noise [15]. Higher frequency vibrations ( $> 100$  kHz) are less susceptible to these effects and are referred to as acoustic emission (AE) [1]. AE is typically measured using a piezoelectric sensor mounted either to the workpiece or on the machine near to the spindle [6]. Due to the high frequency of AE,

preprocessing of the signal is commonplace. This preprocessing consists of filtering, and analog calculations of the RMS value of the signal [5], [6].

### 2.2.2. Feature Extraction for Drilling

Raw sensor signals from TCM systems contain a plethora of data, not all of which is useful for determining tool condition. Features should be extracted that give the maximum amount of information about the tool condition independent of other machining properties. Features can be broken down into three main categories: time domain, frequency domain, and time-frequency domain features. The time domain features consist of moving averages, maximum values, counts above a limit, and RMS signals. Frequency domain signals consist of fast Fourier transforms (FFT) and power spectrum density (PSD) calculations. Time-frequency domain features used for drilling primarily consist of wavelet analysis although the type of wavelet transform used varies from paper to paper [5].

While most of these features have been tested on all signals acquired, certain combinations of sensors and features yield more information about tool condition than others. The following combinations (shown in Table 1) were found to be the most successful for determining the tool condition.

**Table 1: Most common signals measured to infer tool condition**

<b>Signal</b>	<b>Feature Relating to Tool Condition</b>	<b>Study</b>
<b>Spindle motor current/torque</b>	Maximum spindle torque	[1], [9], [16], [20], [21], [25], [30]–[37]
<b>Feed motor current/force</b>	Maximum axial feed force	[1], [9], [11], [14], [16], [20], [30], [33]–[37]
<b>Piezoelectric AE sensor</b>	Max RMS AE	[9], [15], [19], [20], [23], [27], [38], [39]
	Wavelet transform	[23], [40]–[43]

### **2.2.3. Classification Methods for Drilling**

A full spectrum of methods to classify tool condition from raw data and extracted features has been researched. These methods range from simple rule-based upper limit methods to complex artificial neural networks (ANNs) and other machine learning methods. One of the primary issues with research into TCM is that the majority of classification systems lack a systematic way to tune the system to a particular set of cutting conditions, material properties, and tooling used [6]. Machine learning algorithms are one way to overcome this issue. Studies that show that machine learning methods (including ANNs) can yield better classification rates than rule-based methods. The cost of this increased classification accuracy is increased system complexity, system cost, increased training times, and system reliability [5]. Because of these downfalls of ANN based TCM systems, these systems have not yet seen use in industry [6], [44]. Rule based methods (eg: stop drilling after X crosses a predefined threshold) have been successfully used by industry but lack the accuracy of the more complex machine learning systems and often result in TCM systems incorrectly detecting failures.

### **2.3. Industrial Applications of TCM**

Industrial applications of TCM systems are commonplace in high volume production facilities and are slowly migrating into smaller scale machine shops. Modern manufacturing machines and stations ship with basic TCM capabilities that help the operator make better decisions about when to change the tool. In addition to these stock systems, aftermarket TCM systems capable of monitoring tool wear and breakage as well as optimizing the cutting conditions are also available. These systems typically measure spindle power, torque, and force. Most of these aftermarket systems use rule-based models to determine when a tool has worn or broken. These models require a training set of data to determine the upper limits of each variable being monitored for each tool used. It is unlikely that TCM systems will be found in machine shops filling custom, small quantity orders until a method is found for reducing or eliminating the training times required for the TCM system to work.

### 3. Research Objectives

The aim of this project was to develop an indirect TCM system capable of detecting tool breakage (also referred to as insert breakage) in large diameter indexable drills. Specifically, this research focused on using a Sandvik Corodril 880 drill body with inserts to drill holes in 2205 duplex stainless steel plate that are greater than 25 mm in diameter – a process common at MHPS. As this was a continuation of research started by Griffin, [1], these parameters were chosen to be as similar to his research as possible. Griffin stated that a limitation of the TCM he developed was its inability to detect insert breakage [1]; this new research aimed to remedy this inadequacy by running a TCM system capable of detecting tool breakage alongside of his existing TCM system.

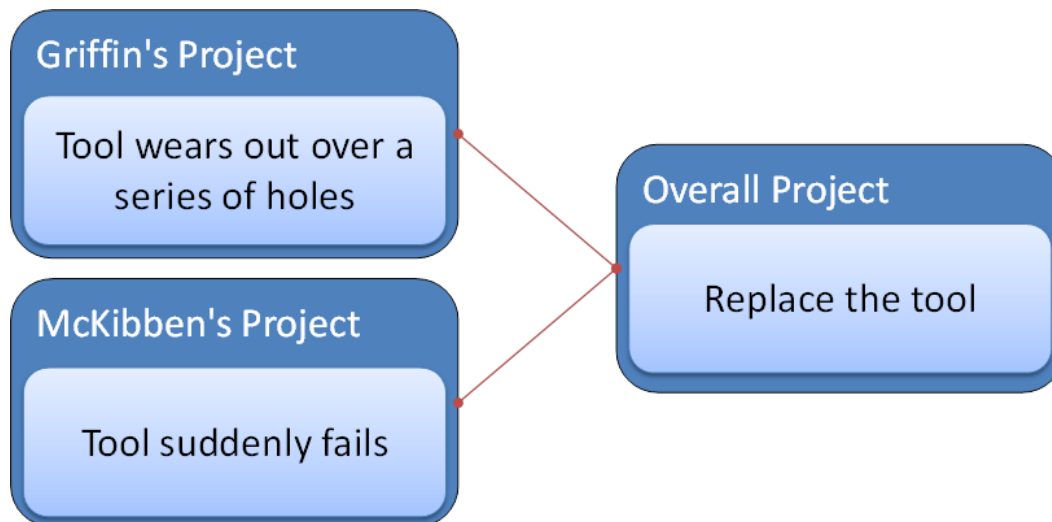


**Figure 3: Development of overall project at MHPS**

A parallel configuration of Griffin’s monitoring system with the one developed in this project allows for monitoring of tool wear and hole diameter as well as detection of tool breakage. This configuration is shown graphically in Figure 3. The specific research objectives for this study are outlined below.

#### **Add AE sensors to existing force sensing capabilities**

In order to capture more information about the tool state, AE sensors were added to the milling machine. The machine is already equipped with current sensors on the spindle motor and z-axis

(coincident with drill axis) feed motor to measure spindle torque and feed force respectively. AE sensors were chosen as the literature has shown that these sensors are useful for detecting tool breakage both of small diameter twist drills and of inserts used in turning and milling operations [5]. As indexable insert drills are a combination of the shape of a twist drill with the cutting inserts of an end mill or turning tool, it was expected that AE will give valuable information about the condition of tools on an indexable insert drill. Sensor placement on the spindle of the machine as well as directly on the workpiece was tested to see the effects of sensor location on signal attenuation. These signals were sampled fast enough to ensure that time-frequency analysis is possible.

### **Develop a TCM system capable of detecting tool breakage and preventing catastrophic failure**

In order to diagnose a broken tool, data needed to be collected for both broken and unbroken tools. Currently, no such data exists for large diameter indexable drills, so new experiments were needed. These experiments needed to collect data for both *good* holes (holes that are within tolerance and drilled with unbroken tools) and *bad* holes (holes where the tool breaks during drilling) so differences can be examined. Once data was collected, signal features were analyzed to find the features that show the most significant change from good holes to bad holes. These features were then used by a variety of classifier algorithms to determine which method provided the best results.

## **4. Experiment Design**

In order to develop a model capable of detecting sudden tool failure, an experiment was designed to collect data for developing and training a model and for testing the new model. Data from a large number of naturally occurring sudden failures was needed in order to develop a model capable of identifying these failures. To collect this information, thousands of holes were drilled into duplex stainless steel plates and the spindle torque, feed motor force, and AE from both the spindle and workpiece were monitored. Tool inserts were used well past the recommended life span in order to achieve the maximum amount of sudden tool failures for the number of holes drilled.

### **4.1. Experiment Parameters**

Experiment parameters, such as spindle speed, feed rate, drill type, insert grade and geometry, coolant pressure, and machine specific properties were chosen to simulate an actual drilling application, namely drilling holes in tube sheets for tube-in-tube heat exchangers, and can be found in Table 2. Specifically for this project, these parameters were chosen to closely replicate Griffin's experiments as the new model developed in this research should complement Griffin's existing wear model. Limited research has been done investigating the differences in TCM system responses to varying materials and cutting conditions so all attempts were made to have the same experimental parameters as Griffin used to allow for both Griffin's model and the new model developed to function properly on the machine at MHPS. One key change that was made from Griffin's research was the use of a smaller diameter drill. This new tool was from the same series of drills that Griffin used (Sandvik Corodril 880) however, a smaller diameter (26 mm instead of 39 mm) was chosen to allow more holes to be drilled in the limited amount of material in order to gather more raw data.

**Table 2: Drilling parameters used for testing**

<b>Parameter</b>	<b>Value Used For Testing</b>
<b>Machine</b>	Toshiba BF-130A Horizontal Boring Mill MHPS Machine 'BF-3'
<b>Spindle speed</b>	98 m/min for middle of hole 55 m/min entry into hole 65 m/min exit from hole
<b>Feed rate</b>	0.130 mm/rev
<b>Coolant pressure</b>	700 psi Through tool and flood coolant
<b>Drill body</b>	Sandvik Coromant CoroDrill 880 Both 39 mm and 26 mm diameters used
<b>Material</b>	2205 Duplex Stainless Steel 38.1 mm thick Mounted to concrete backing block Plywood backing plate See Figure 6 for geometry

Due to the smaller diameter tool and the limitations of the horizontal boring machine (HBM) used, the machine could not spin the smaller drill fast enough to achieve the same surface cutting speed used in Griffin's research (130 m/min). Due to the spindle speed limitation, the inserts used in this experiment have a slightly higher chip load than those used by Griffin.

## **4.2. Experimental Apparatus**

### **4.2.1. Machine Setup**

All experimental data was collected at the Saskatoon location of Mitsubishi Hitachi Power Systems Canada Ltd. (formerly Hitachi Power Systems Canada Ltd.) on a Toshiba BF-130A HBM designated BF-3. This machine was equipped with high pressure, through the tool, coolant running at 700 psi for all tests. The same machine setup was used for experiments conducted by

Griffin. Figure 4 shows a schematic drawing of the HBM setup used for drilling tube sheets – a typical drilling intensive manufacturing process done at MHPS on BF-3. Also shown are approximate locations of the built in current sensors for determining the spindle motor and feed motor power. The workpiece and workpiece mounting scheme shown in Figure 4 are typical for drilling tube-sheets or baffle-plates for tube-in-tube heat exchanges but differ from the setup used for testing. A more exact schematic of the setup, along with AE sensor positions can be found below in Figure 5. Note the plywood backing not present in the mounting scheme shown in Figure 4.

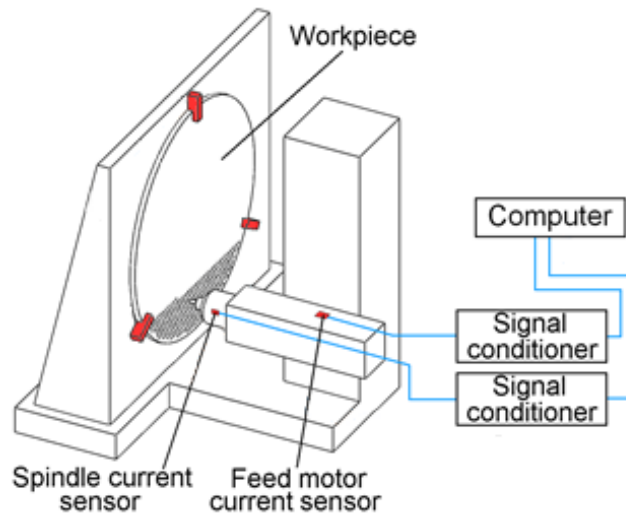


**Figure 4: Schematic of HBM used for testing with built in sensors**

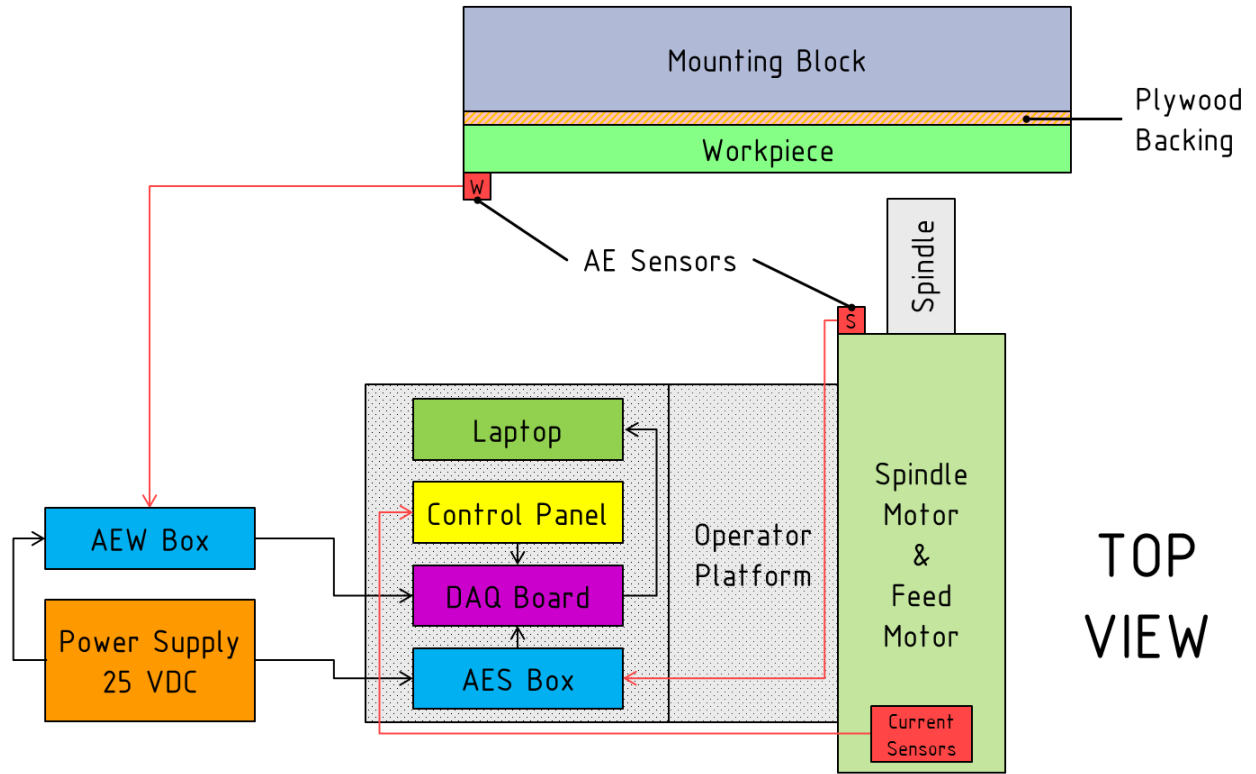


**Figure 5: Schematic top view of experimental setup**

Figure 5 also shows the signal paths of all sensors to the data acquisition system (DAQ). The AE sensors for both the workpiece (AEW) and the spindle (AES) both pass through a conditioning box before reaching the DAQ. This conditioning box provides power to the sensor and sends two signals to the DAQ - an AE RMS signal and a high pass filtered signal. All the signal abbreviations used are denoted as shown below in Table 3.

**Table 3: Signal abbreviations**

Signal Abbreviation	Signal Description
<b>T</b>	Current signal from spindle (Torque)
<b>F</b>	Current signal from feed motor (Force)
<b>AESF</b>	Filtered output of the AE signal from the spindle
<b>AESR</b>	RMS output of the AE signal from the spindle
<b>AEWF</b>	Filtered output of the AE signal from the workpiece
<b>AEWR</b>	RMS output of the AE signal from the workpiece

### 4.2.2. Material

Holes were drilled into pieces of 31.8 mm thick 2205 duplex stainless steel. Three separate workpieces were used over the course of the testing to drill 2251 holes, 663 on the first plate and 794 on each of the later plates. These workpieces were leftover from actual tube sheet manufacturing so their material properties are identical to that of tube sheets, however, their geometry was different. The pieces of duplex used were the corners cutoff from the circular tube sheets (seen mounted in Figure 4) and measured roughly 2 m tall and wide. More exact geometry of the workpieces used for this testing can be seen in Figure 6.

Workpieces were clamped to a vertical backing block in four places to hold the workpiece for drilling. Clamping the workpiece was chosen over bolting the workpiece onto the backing plate using standoffs (standard practice for tube sheet manufacturing) due to the smaller size of the workpiece and due to machine time constraints. Plywood was used instead of standoffs to separate the workpiece from the metal backing plate to avoid damaging the machine when it broke through the workpiece.

Figure 6 shows how the workpiece was attached to the backing block. The left half of the image shows the first workpiece clamped in place (three of the clamps can be seen) and ready to be drilled. The right side of Figure 6 shows the third workpiece being removed from the backing plate after drilling. Three of the loosened clamps can be seen as well as the pattern of holes drilled through the workpiece.



**Figure 6: Workpiece mounting and hole pattern**

### **4.1.3. Tooling**

This project used indexable insert drills supplied by Sandvik Coromant. The drill bodies were 39 mm and 26 mm models from the CoroDrill 880 series (the same series as Griffin used). Inserts used for this project varied in both geometry and material grade. The geometry of the insert is denoted by the first two letters of the part number and the material grade is identified by the last four numbers (ex. XX1234 would denote an insert with geometry XX and material grade 1234). Details on the insert grades used can be found in Sandvik's website. Note that when looking up the actual part numbers of inserts size information is needed; as only one size of insert fits each of these drills (one size for the 39 mm and a smaller size for the 26 mm) this size information has been omitted from this report for simplicity.

The inserts used with the 39 mm drill were the same ones used by Griffin's research and consisted of LM4024 outer inserts and GM1044 inner inserts. These inserts are the recommended inserts for the 39 mm drill body when drilling duplex stainless steel. Inserts for the 26 mm drill were chosen to closely replicate the inserts used in Griffin's research. However, due to the smaller drill body and higher chip load (caused by spindle speed limitations), slightly different inserts were chosen as the recommended insert geometries and grades for drilling duplex with the 39 mm drill were not the same for the 26 mm drill. Inner inserts used with the smaller drill bodies were GR1044 for all tests. When compared to the GM geometry inserts used with the large drill, the GR geometry has a slightly larger corner radius and chip-breaker relative to the size of the insert. This larger relative geometry means that the corner radius and chip-breaker length are very similar in absolute size between the larger GM and the smaller GR inserts. Different grades and geometries of outer inserts were used throughout the testing. These outer inserts were chosen to both replicate Griffin's results and also to try and induce more natural failures to occur. The outer inserts used throughout the testing were: GR4024, LM4024, GM4014, and LM4014.

#### **4.2.4. Sensors and Sensor Placement**

##### ***4.2.4.1. Torque & Force Sensors***

Two current sensors were used to measure the spindle motor current and feed motor current. The current sensor from the spindle motor was built into the machine and output a voltage from 0-10 VDC proportional to the spindle current. The feed motor current sensor was installed as part of Griffin's research and was an Ohio Semitronics CT8-017D RMS current sensor. The feed motor sensor was also calibrated to have a 0-10 VDC output based on the feed motor current. Both of these sensors were chosen so that the maximum current would not be out of the measurement range of the sensor. The calculation to convert these current readings to torque or force was never conducted. Although AC motor current and power generated do not necessarily share a linear relationship, the relationship between current and power has a one-to-one relationship where more current flow causes increased motor power. Because of this current-power relationship, the raw readings from the current sensors (VDC) were used to simplify the analysis; as neither of these sensors were calibrated in terms of power and neither the internal resistance nor applied voltage was recorded, spindle power and feed motor power will be presented in units

of VDC. As these signals are only used within the model, this simplification will not hinder analysis. If a physical model, opposed to a phenomenological model, were to be developed, it may be beneficial to calibrate both the spindle and feed motor sensors to units of power (W) and force (N).

#### **4.2.4.2. Acoustic Emission Sensors**

Two AE sensors were used to collect information about the drilling operation. Both of the sensors used were Kistler 8152B111 AE sensors each running through a Kistler Piezotron Coupler Type 5125 operating at 25 VDC. The couplers pre-conditioned the AE signals and fed both RMS and filtered values (through an internal high pass filter) to the DAQ.

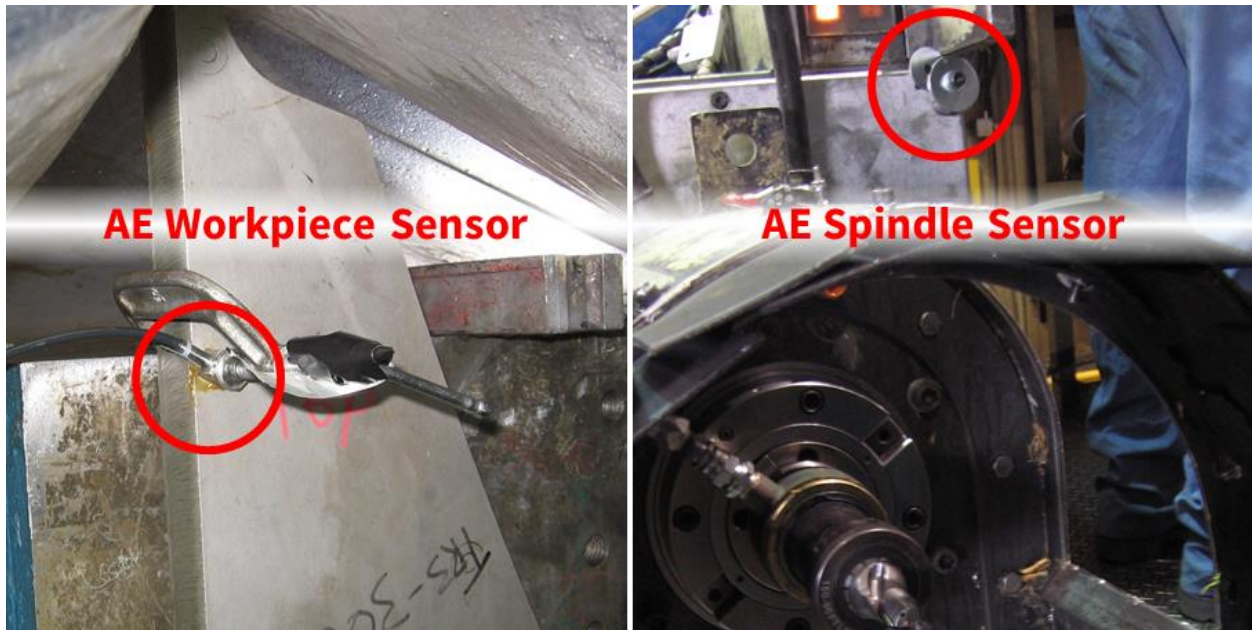


**Figure 7: AE sensor mounting locations**

One of the AE sensors was mounted directly to the workpiece (AEW) and the other was mounted on the machine as close to the spindle as possible without impeding machine operation (AES). The AEW sensor was originally mounted 575 mm from the top of the workpiece. After hole 503 on the first workpiece the AEW sensor was moved up to 200 mm from the top of the workpiece so the spindle would not collide with it; this new placement can be seen if the left half of Figure 7.

When the AEW sensor was moved further from the point of drilling, the data was checked to ensure that there was no significant difference in signal from the AEW sensor due to improper mounting or unwanted attenuation. After moving the AEW sensor, some signal features increased while others decreased. Due to the large variance in the signals and other factors affecting signal magnitude, it is difficult to determine if signal attenuation caused by drilling at varying distances from the sensor is a significant factor in signal magnitude. These AEW data can be seen below in Figure 8 – the first 71 holes plotted were drilled before the AEW sensor was moved and the rest of the holes were drilled after the sensor was moved up the workpiece.

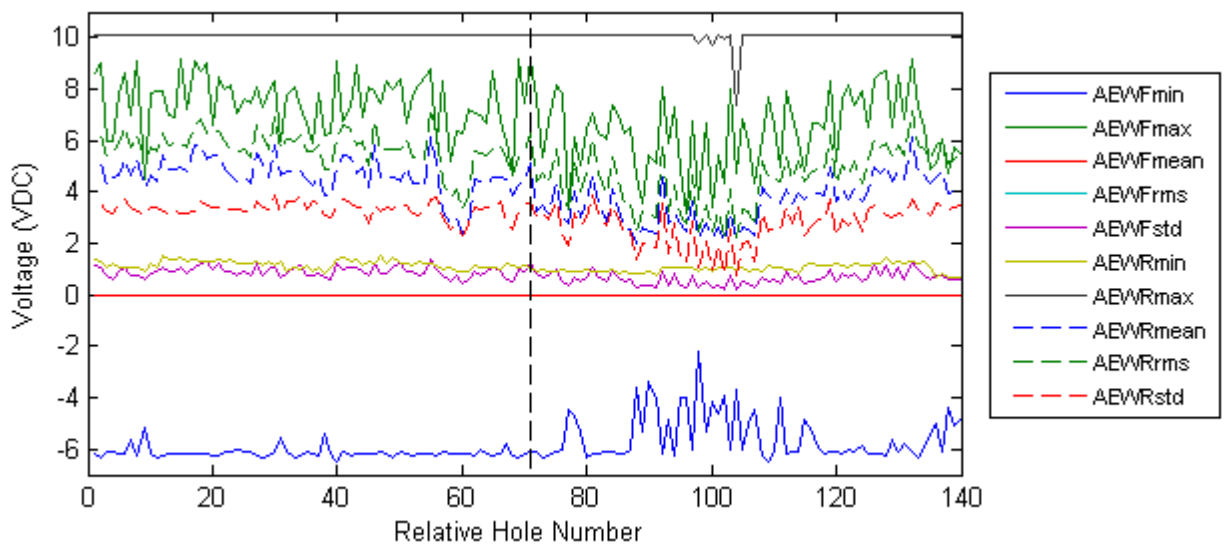


**Figure 8: Plot of all AEW features shown before and after moving the AEW sensor**

It's interesting to note that the repositioning of the AEW sensor increased the variance of all features except for AEWfmean. This increased variance could be due to mounting the sensor on a less rigid part of the workpiece – closer to the unsupported top corner.

Due to slight differences in the mounting of each of the three workpieces used, the AEW sensor was in slightly different locations relative to the holes drilled, but it always remained 200 mm from the top of the workpiece. The spindle AE sensor, shown in the right of Figure 7, was mounted just outside of the spindle guard as close to the tool as possible (the drill can be seen in the lower right of Figure 7) and was never moved or adjusted over the course of the experiment.

### **4.2.5. Data Collection**

All data was collected through a National Instruments USB-6315 data acquisition board (DAQ) to a custom software interface in MATLAB 2014a. Figure 5 shows a general wiring schematic of these systems. Data was collected at the maximum possible speed for this interface, 1.667 MHz (10 MHz maximum for the device split to 6 channels of data sampled simultaneously), in order to minimize aliasing should frequency analysis of the AE signals be conducted.

Due to the long cable runs required to connect DC power and the workpiece AE sensor to the DAQ on the operator platform, minimizing electrical noise on the sensor signals was a priority when wiring up the sensors. All cable runs from the AE sensors were run in 50  $\Omega$  coaxial cables grounded to only the DAQ. These cables were selected based on specifications from the AE signal condition boxes to decrease the amount of signal reflection caused by mismatching cable impedances. In addition, all signal inputs were run through differential input channels on the DAQ to make use of common mode rejection to further diminish the effect of electrical noise picked up in the long cable runs.

To minimize noise due to ground loops, all sensors were only grounded directly to the ground plate on the DAQ. In addition, the 25 VDC power supply used to power the AE sensor condition boxes was also only grounded to the DAQ. The cables connecting the current sensors used to monitor the spindle and feed motor were internal to the machine and were grounded to both the machine frame as well as the DAQ ground. However, as frequency analysis will not be conducted on either of the current signals, any noise due to ground loops in those signals will be filtered out.

## **4.3. Experimental Procedure**

### **4.3.1 Experimental Setup**

To ensure that sudden failure data collected from these experiments was compatible with (statistically similar to) the wear data collected by Griffin, an initial run of holes using standard tube sheet drilling parameters was carried out. This run used identical parameters to Griffin's control tests, however the method used to mount the workpiece was slightly different. The test used a 39 mm CoroDrill 880 drill with LM4024 outer inserts and GM1044 inner inserts at a feed

rate of 0.130 mm/rev and a surface speed of 130 m/min and ran for 96 holes. Data from this initial set of holes was found to be similar to data collected by Griffin and worked with all algorithms developed by Griffin. This similarity shows that the plywood backing plate had a minimal effect on the overall data set. Data from this portion of the experiment were not used for training or testing classifiers but were collected to confirm that all sensors were working properly. As no research has been conducted correlating differences in torque, force, or AE between different diameters of indexable insert drills, data collected from these initial 96 holes will not be used for any further analysis.

### **4.3.2. Collecting Testing Data**

After the initial 39 mm drill testing, a baseline set of data for the 26 mm diameter drill was collected. This baseline data was collected using a 26 mm CoroDrill 880 drill body with GR4024 outer inserts and GR1044 inner inserts at a feed rate of 0.130 mm/rev and a surface speed of 98 m/min and ran for 370 holes. Data collected from these holes will be used for testing models that have been trained with other data.

#### ***4.3.2.1. Chip Definition***

For the purposes of this research a chipped insert was defined as an insert that is missing a piece of material large enough to detect with the human eye. While chips smaller than 0.2 mm wide still might be detectable by the naked eye, no chips this small were found after examining the inserts after testing was completed.

### **4.3.3. Commissioning a Method to Force Failures**

To ensure the efficient use of materials in experiments, different inserts and machine parameters were tested to speed the process of tool breakage. Naturally occurring, sudden tool failure only occurs about once every 100 holes. If a method could be found to speed the process of tool breakage, the average number of holes needed to break a tool could be reduced and more training data could be collected. Data collected from forced failures must closely resemble data collected from natural failures in order for forced failure data to be useful for model training. Table 4 contains all combinations of tooling (inserts) and machine parameters (feed rate and calculated chip load) tested in an attempt to find a method of forcing insert failure with data that closely resembles naturally occurring failures. Note that the feed rates shown were used for the entire

hole and no slower entry or exit feed rates were used for these tests. Of the outer inserts used, the GR geometry is the strongest, followed by GM and LM; also, 4024 is a tougher grade of insert than 4014. The inner insert (GR1044) was never changed throughout the testing. The spindle was running at its maximum speed of 1200 rpm (98 m/min surface speed with a 26 mm drill) for all tests.

**Table 4: Machine parameters tested for forced natural failures**

<b>Outer Insert</b>	<b>Feed Rate (mm/min)</b>	<b>Chip Load (mm/rev)</b>
<b>GR4024</b>	234	0.195
	312	0.260
<b>LM4024</b>	288	0.240
	312	0.260
<b>GM4014</b>	288	0.240
	312	0.260
<b>LM4014</b>	288	0.240
	312	0.260
	375	0.313
	450	0.375

The parameters shown in Table 4 were tested in the order shown – using increasingly brittle inserts at higher chip loads. As the spindle speed was held constant for all trials, the chip load was increased solely by increasing the feed rate of the drill. Each insert and feed rate combination was tested for a small number of holes (5-20). After these holes were drilled and if no failure had occurred, a fresh insert was installed and a different feed rate was tested. None of the trials, except for the 450 mm/min LM4014 trial, resulted in insert failure. The final trial instantly resulted in catastrophic failure of the outer insert and damaged the drill body beyond repair.

The damaged drill from the first hole of the 450 mm/min test can be seen in the right of Figure 9. An undamaged drill body is shown on the left of Figure 9, and the damaged drills body has a red outline representing where the body used to exist. Note that all material circumferentially behind

the outer insert was sheared off after the outer insert broke off and before the operator could stop the machine. While this failure resulted in a useful training data point, the project budget would not allow the breakage of a drill body for each data point. In addition to budget constraints, data collected from this catastrophic failure was significantly different from data collected from naturally occurring tool breakage, making failures such as this unideal for training data.

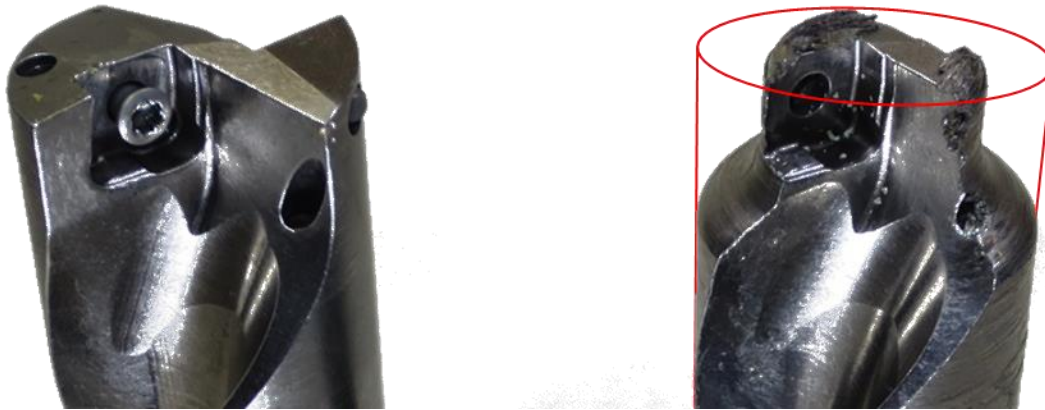


**Figure 9: Comparison of undamaged (left) and damaged (right) drill body end**

#### **4.3.4. Collecting Training Data**

As it was discovered that methods of forcing tool failure by varying inserts or feed rate did not result in useful training data as no method reliably caused the inserts to break, the rest of the material available for testing was simply used to collect training data from naturally occurring failures. Usable data was collected for a total of 2062 holes using a 26 mm CoroDrill 880 drill body with GR4024 outer inserts and GR1044 inner inserts at a feed rate of 0.130 mm/rev and a surface speed of 98 m/min – the same setup used for collecting test data. This data was stored in binary (.BIN) files for later analysis.

Holes were drilled in sets of 1 to 7 holes before stopping to inspect the inserts. If at any point the operator or researcher thought an insert might have chipped, the drill was stopped after the current hole and the inserts were examined. While it may have been beneficial to stop the drill inspect the inserts after every hole, time restraints dictated larger groups of holes be drilled between stops.

If an insert was found to be chipped, it was replaced by either a new insert or rotated to a fresh cutting edge (each insert has 4 cutting edges that don't wear when not in use). If an insert was worn past what would typically be acceptable in a production environment, it was still used. Only inserts that were worn so much that further drilling would cause damage to the drill body were replaced. This method of replacement meant that a worn insert could be paired with a fresh insert in the other location on the drill body – i.e. worn outer paired with a fresh inner insert.

At the start of each new run (there were 6 different runs), and also a few times in the middle of some of the longer runs, both inserts were replaced at the same time. By doing this joint replacement, information on a pair of fresh inserts was collected and could be compared to a worn/fresh pair in future research.

## 5. Algorithms Developed and Data Analysis

### 5.1. Hole Drilling Cycle

The process of drilling a hole in the workpiece was divided into numbered states according to the physical properties of the drilling cycle. By dividing each hole into states, more specific information could be extracted from each of states and thus used by the classifier models. The definitions of states in a drilling cycle are provided in Table 5.

**Table 5: Definition of states of a drilling cycle**

States	Definition
1	Not in drilling cycle
2	Feed in
3	Drill entrance
4	Steady state at slow feed rate
5	Increasing feed rate
6	Steady state drilling
7	Drill exit
8	Retract from hole

MHPS uses a multi-feed-rate drilling process to elongate the life of their tools. This procedure is outlined below and can be visualized, by observing torque (green) and force (blue) data, in Figure 10:

- With the spindle running, advance the drill towards the workpiece at an initial feed rate of 65 mm/min
  - The cutting edge makes contact with the workpiece at the transition between state 2 and 3 as seen by the increase in spindle torque
- Once the cutting edges of the inserts are fully immersed in the workpiece (depth of about 2 mm), increase the feed rate to the programed value of 98 mm/min

- State 4 occurs as the drill reaches a steady state at this initial feed rate. The increased feed rate marks the transition between state 4 and 5
- Once close to the back of the workpiece (about 3 mm of material left), decrease the feed rate to 55 mm/min
  - This change in feed rate happens at the transition between state 6 and 7

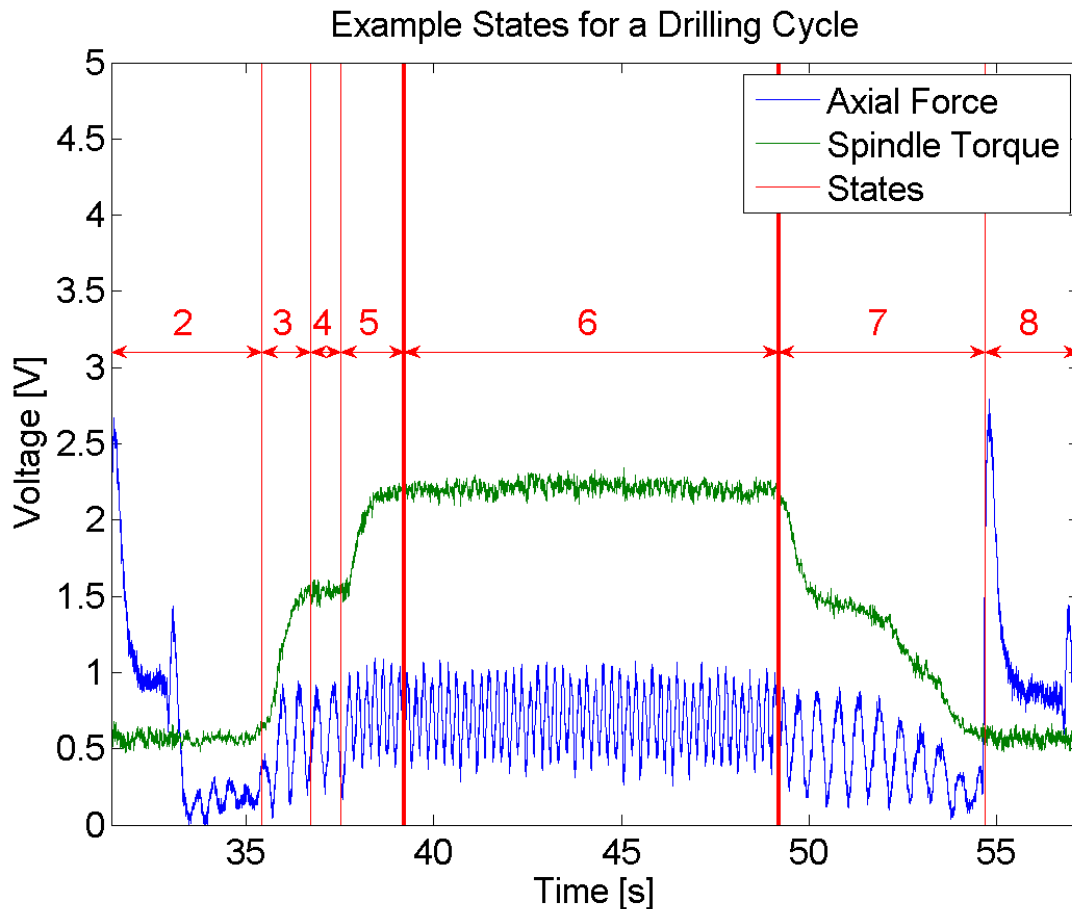


**Figure 10: Drilling states for a single hole**

Slowing down the feed rate for workpiece entry and exit is standard procedure at MHPS as they have found it to reduce the number of catastrophic failures that occur. Although some tests were done to see the effects of altering this drilling algorithm (see section 4.3.3. Commissioning a Method to Force Failures) the final data set used the above drilling process for all holes.

Although these states could be identified by interfacing with the G-code running the machine, they were instead calculated based on the torque and force signals as no G-code interface was available during testing. This method of calculating states requires less data collection equipment and data processing than interfacing with the G-code and also gives more accurate results for state transition times that could be achieved using G-code alone – this method can detect exactly when the drill enters the workpiece whereas G-code might be slightly off.

### **5.1.1. Algorithm to Identify the Process of Drilling a Hole**

In order to extract features from the drilling process, an algorithm was developed to identify the drilling of each hole from data collected. This algorithm uses the spindle torque and feed force data to identify the start and end of the drilling cycle for each hole.

As shown in Figure 11, the hole finding algorithm divides holes into 3 of the 8 possible states: 1 – not in drilling cycle, 2 – feed in, and 8 – retract from hole. Everything classified in state 2 by the algorithm is further classified into states 2 through 7 by the hole division algorithm and everything classified as either state 1 or 8 will not change. The hole finding algorithm works by identifying spikes in the axial force signal and uses these points to determine which way the drill is moving. From either state 1 or 8, a spike in axial force (generated by beginning to move the spindle) combined with a high spindle torque after the force spike signals a transition into state 2. From state 2, a force spike after a minimum time has passed signals another change in axial direction of the spindle (retracting from the hole) and the transition to state 8. After a complete cycle has been identified (ending in state 8) the hole will be saved so it can be divided further by the hole division algorithm.

Figure 11 makes use of a few tunable Boolean operators. Tuning of these variables allows for the find hole algorithm to be used on a variety of different drilling cycles. These operators are described in Table 6.

**Table 6: Boolean operators used in the find hole algorithm**

<b>Boolean Operator</b>	<b>Definition</b>
<b>ForceSpike</b>	True if a force spike is found, else false
<b>LowForceBefore</b>	True when the average force, over a short window of time, before the current data point is below a given threshold, else false
<b>HighTorqueAfter</b>	True when the average torque, over a short window of time, after the current data point is above a given threshold, else false
<b>MinTime2to8</b>	True once the minimum allowable time to drill a hole has passed, else false
<b>HoleSaved</b>	True when the current hole has been saved, false when current data point belongs to an unsaved hole

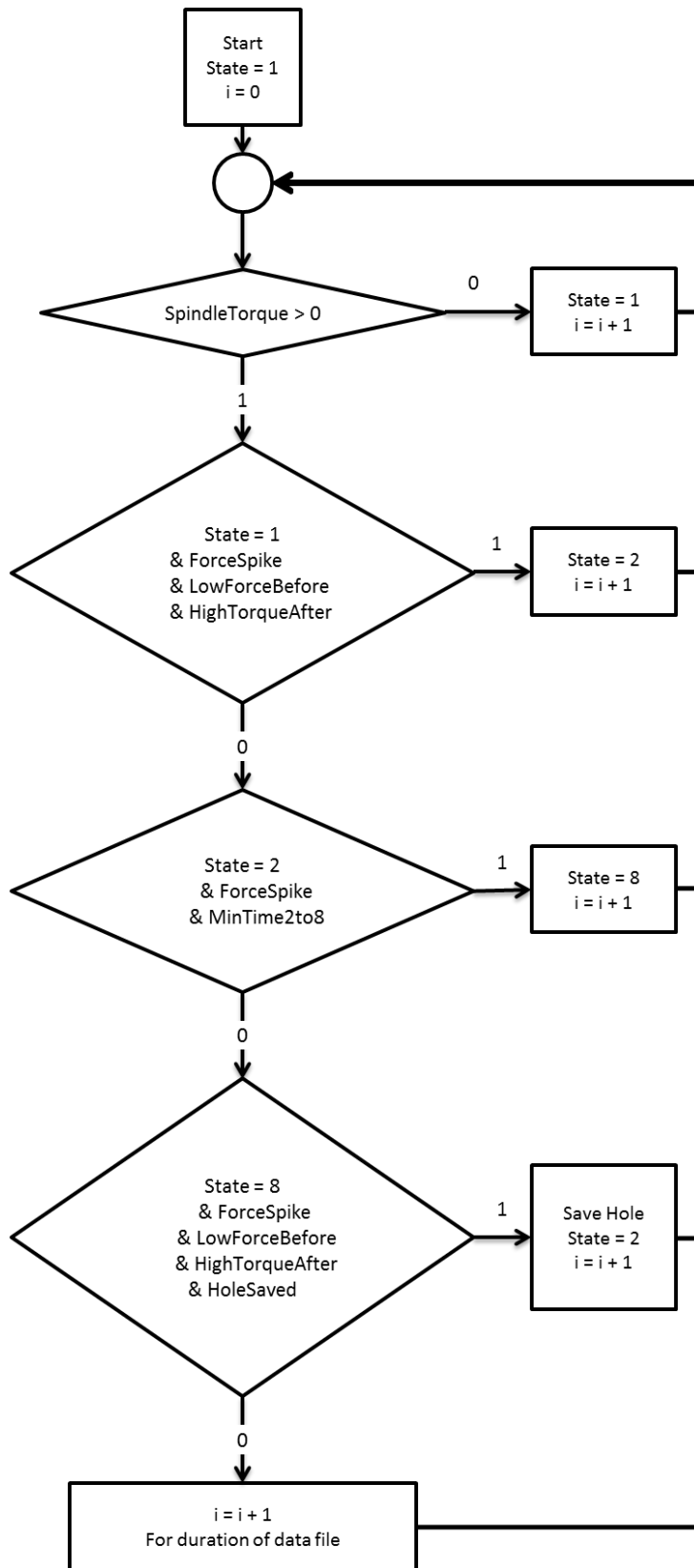


**Figure 11: Flow chart of the algorithm to identify the proces of drilling a hole**

In order to ensure correct state classification, this algorithm looks forward to calculate the average torque after a force spike. Due to the foresight required, this algorithm is not well suited for on-line monitoring of drill state. If such an algorithm was needed, it would be best to tie into the G-code to determine the axial direction and speed of the spindle in real-time.

Due to the high sampling frequency of the data collected, a few minor changes were made to speed up the identification process. One of these changes was that the ForceSpike Boolean only looked for force spikes above a threshold level. Also, the other Boolean variables were not calculated until a force spike was identified. These changes significantly increased the speed and efficiency of the hole identification process.

### **5.1.2. Manual Alignment of Hand Recorded Data**

After the hole-finding algorithm was completed, the manually collected data containing information on tool breakage was inputted. To obtain meaningful results, it was critical that the identified holes lined up perfectly with the manual data. As the hole finding algorithm only correctly classified 99.2% of holes, there were a number of holes that went unidentified. As it's difficult to tell which holes went unidentified, each identified hole was plotted and lined up with the manually collected data sure ensure the correct holes were omitted.

### **5.1.3. Hole Division Algorithm**

After every hole was identified and paired with the manually collected breakage data, each hole was divided into multiple states so features could be easily calculated. The division algorithm used split states based on the torque, force, and the first and second derivative of the torque signal after it had been down-sampled to 2.0 kHz and run through an A-B filter. The basic process for dividing the holes is shows below and outlined in Figure 12:

- An  $\alpha$ - $\beta$  filter was applied to the torque signal to further smooth out the data
  - This additional filter was needed as the derivatives of the torque signal after only the moving average filter are still very sporadic
- The first and second derivatives of the  $\alpha$ - $\beta$  filtered torque data were calculated
  - Defined as Tdx and Tdx 2 respectively

- Approximate threshold values for the second derivative were calculated using the variance of the 1<sup>st</sup> derivative
  - Defined as ULim and LLim for the upper and lower limits
  - These threshold values were just a starting point for tuning the hole division algorithm and they were further adjusted by a scalar
- Each time the 2nd derivative of the torque crossed the threshold was an indication of a significant change in the spindle torque and a change in the state
- To improve the robustness of the algorithm, timers were used to prevent rapid transitions between states that could occur due to noise in the derivative signals
  - The timers *minTime* and *minTimeState6* were used and tuned to prevent these type of errors

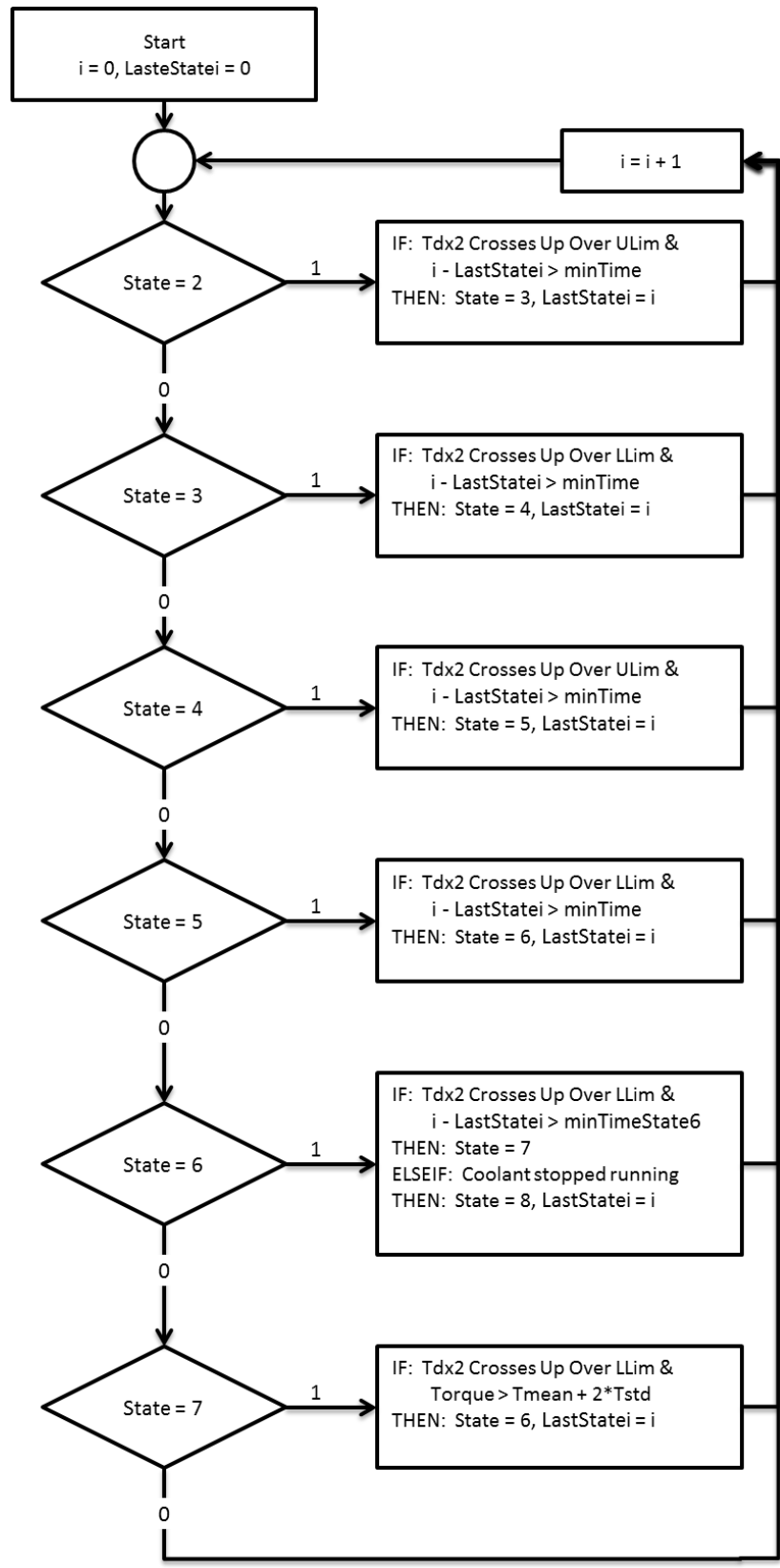


Figure 12: Flow chart of the algorithm to divide the proces of drilling a hole

#### **5.1.4. Time Domain Feature Extraction**

After every hole was identified and divided into states, time domain features were calculated for the steady state drilling portion (state 6) of each hole. A total of 30 time domain features were calculated. The time domain features investigated were the minimum, maximum, mean, RMS, and variance. Each of these 5 features was calculated for all 6 of the collected signals: torque, force, spindle and workpiece AE (both the RMS and filtered signals). All features along with their assigned feature number (for ease of coding) are show in Table 7. These features were chosen as previous research into detecting tool breakage (mainly in small diameter twist drills) has shown that these features can contain information about the health of the drill. Once calculated, these features were used as inputs to the classifier models developed to detect tool breakage.

**Table 7: Values assigned to each feature**

<b>Feature Number</b>	<b>Signal</b>	<b>Feature</b>
1	Torque	Minimum
2	Torque	Maximum
3	Torque	Mean
4	Torque	RMS
5	Torque	Standard Deviation
6	Force	Minimum
7	Force	Maximum
8	Force	Mean
9	Force	RMS
10	Force	Standard Deviation
11	AESF	Minimum
12	AESF	Maximum
15	AESF	Mean
14	AESF	RMS
15	AESF	Standard Deviation
16	AESR	Minimum
17	AESR	Maximum
18	AESR	Mean
19	AESR	RMS
20	AESR	Standard Deviation
21	AEWF	Minimum
22	AEWF	Maximum
23	AEWF	Mean
24	AEWF	RMS
25	AEWF	Standard Deviation
26	AEWR	Minimum
27	AEWR	Maximum
28	AEWR	Mean
29	AEWR	RMS
30	AEWR	Standard Deviation

### **5.1.5. Generate Experiment Object**

Object-oriented programming was used to readily store information about each individual hole as well as information about each run conducted. The lowest rank of object used was the *Hole* object. This object contained information on each individual hole including the filtered signals, the state of each point and the features calculated for that hole. The *Run* object contains information about each run including run number, relative hole number, and the program hole number (for lining up holes with the G-code and manually collected data). Each *Run* object also contains all the *Hole* objects for every hole in the run.

As *Run* objects are very large (they contain *Hole* objects which contain huge amounts of raw data), *RunSummary* objects were created for use in analysis. These *RunSummary* objects contain all the same information as the *Run* and *Hole* objects except for the raw and filtered data. By eliminating unused data from each object, *RunSummary* objects are much more efficient to work with when training and testing classifiers. Lastly, the *Experiment* object simply contains a collection of all *RunSummary* objects for easy access when coding. Each of the objects contains methods for plotting and analysis of data contained in the object.

## **5.2. Modification of Algorithms**

Data for this project was collected at very high frequencies so that future frequency analysis could be conducted. However, the high sampling frequency also resulted in a very large data set (over 925 GB in binary files) which required a long time for processing, even on a fast computer. In order to expedite the analysis of the data for this project, a number of modifications were made to some of the algorithms used. While these changes do not alter the results presented in this study, they will need to be addressed if different analyses are to be run using the collected data with the project code. These changes are outlined and explained in the following sub-sections

### **5.2.1. Down Sampling and Filtering**

In order to more efficiently deal with the large amount of data collected the data was run through a moving average filter and then down-sampled by a factor of 83 to get a sampling frequency of 2.0 kHz. Even with the careful precautions taken to minimize electrical noise in the signal, most

signals collected were too sporadic to interpret before filtering. This high frequency, high amplitude noise was likely caused by the long cable runs necessary to connect the sensors on the large industrial machine. As such, a 1000 point moving average filter was applied to the data to smooth out some of the major peaks and valleys.

One of the main issues with using a moving average filter on a data set is the loss or delay of information. By averaging over a large number of data points, the filtered data lags behind the true average by half the window used. While use of a larger window for the moving average filter could help smooth the data more, 1000 point window was chosen as it smoothed out the data enough to be usable without skewing the time scale significantly due to the high original sampling frequency – the averaged data will lag behind the original by less than 3 ms at the sampling rate of 167 kHz per channel.

To further improve the efficiency of the analysis and decrease code run-time, data was down-sampled. A down-sampling factor of 83 (only use every 83<sup>rd</sup> data point after filtering) was chosen as it resulted in a working sample rate of 2008. Hz which was very close to the rate used by Griffin. Although much of the frequency and time-frequency information is lost in the down-sampling process, time domain information about the drilling operation remains mostly unchanged after this process. As only time domain features are investigated in this report, down-sampling the data set is a very effective way to save time running analysis.

The only feature investigated in the report that is significantly affected by filtering and down-sampling is the variance or standard deviation of the signals. Both the moving average filter and the act of down-sampling will drastically reduce the variance of the signals. However, this reduction in variance does not make it obsolete as a feature; it simply changes what the variance feature calculates. The unfiltered variance of a given signal would mainly provide information on the noise collected as, from observation, the magnitude of the noise was much larger than the mean signal in most cases. Variance of the filtered signal, on the other hand, provides more information about how the mean value of the signal changes over a given state of a given hole. While the calculated variance differs between the filtered and unfiltered signal, both features could potentially carry information on tool breakage.

### **5.2.2. Force Peak Algorithm**

In order to speed up the hold finding algorithm, a modification was made to the axial force peak detection algorithm. In order to find the start and end of each hole, the location of an axial force spike or peak needs to be determined. Typically a peak detection algorithm looks forward and backwards in the data to determine if it has found a local maximum within a certain range. Due to the very high sampling rate and the large number of holes, this algorithm is very time consuming to run.

In order to improve the speed of the axial force peak detection algorithm, this algorithm was only run when values of axial force were above a predetermined threshold. This limit was set after observing the force peak values throughout the data set. The downside of this threshold-based algorithm is that some holes were still not found – this error may be due to other factors as well. After tuning the threshold-based algorithm over 99.2% of holes were correctly found. Also, after implementation of this threshold, the hole finding algorithm was able to find holes over twice as fast – resulting in a time saving of over 30 minutes each time the code was run.

### **5.2.3. Modified Algorithm to Identify the Essential States**

To further reduce the time spent running code, modifications were made to the hole division algorithm to only identify the used states. As the time domain features used in this study were all calculated from the steady state drilling portion of each hole (state 6), the hole division algorithm was modified so that states 4 and 5 were not identified. This modification not only improved the speed of the algorithm, it also improved the accuracy of identifying the start of state 6.

## 6. Classifier Development and Validation

Once features had been extracted from the data, classification models were developed. These classifiers were then tested and compared to each other using confusion matrices. These matrices, shown below, show the output of a classifier for the given testing set of data. The rows of the matrix reflect the actual state of a given point (or a hole for this research) and the columns represent what class the classifier model assigned to that point.

$$C = \begin{bmatrix} \text{Predict Good, Actual Good} & \text{Predict Bad, Actual Good} \\ \text{Predict Good, Actual Bad} & \text{Predict Bad, Actual Bad} \end{bmatrix}$$
$$= \begin{bmatrix} \text{True Positive} & \text{False Positive} \\ \text{False Negative} & \text{True Negative} \end{bmatrix}$$

A perfect classifier has a confusion matrix with values along the main diagonal and zeros in all other locations. However, classifier outputs are rarely perfect and frequently misclassify points. These misclassified points show up as positive numbers not on the main diagonal of a matrix. For this project, there are only two options for errors: false positives (type I error) and false negatives (type II error). False positives happen when the model classifies a given hole as bad when in fact the hole was actually good. If a classifier was being used for live monitoring of a drill, a false positive would trigger the drill to stop and an operator would have to manually check to ensure that the drill was still good. False negatives (or undetected failures), on the other hand, are holes that are actually bad holes but are classified as good holes. This type of failure is much more dangerous than the false positive as drilling with a bad drill can potentially cause catastrophic damage to the drill or workpiece. False positives are much preferred over false negatives, but neither type of error is ideal.

### 6.1. Classifier Selection

As there are a wide variety of classifiers available for use and multiple different classifiers were initially selected and tested to find the classifier that most accurately could detect tool breakage. After all the classifiers outlined in the sub-sections below were tested and cross-validated, the best classifier for the drilling application was chosen.

### 6.1.1. Zero R Classifier

The Zero R classifier is not so much an actual classifier as a baseline test. The simple algorithm for this classifier is as follows:

- Determine most common outcome in training data set
  - For this research, the most common outcome was a good hole
- Assign the most common outcome to all holes in the testing data set

As there are only 2 states a tool can reside in (good or bad), the Zero R classifier is an excellent baseline. This output can also be seen visually in Figure 13; the difference between actual data and the Zero R model for good holes is equal to the number of bad holes in the actual data.

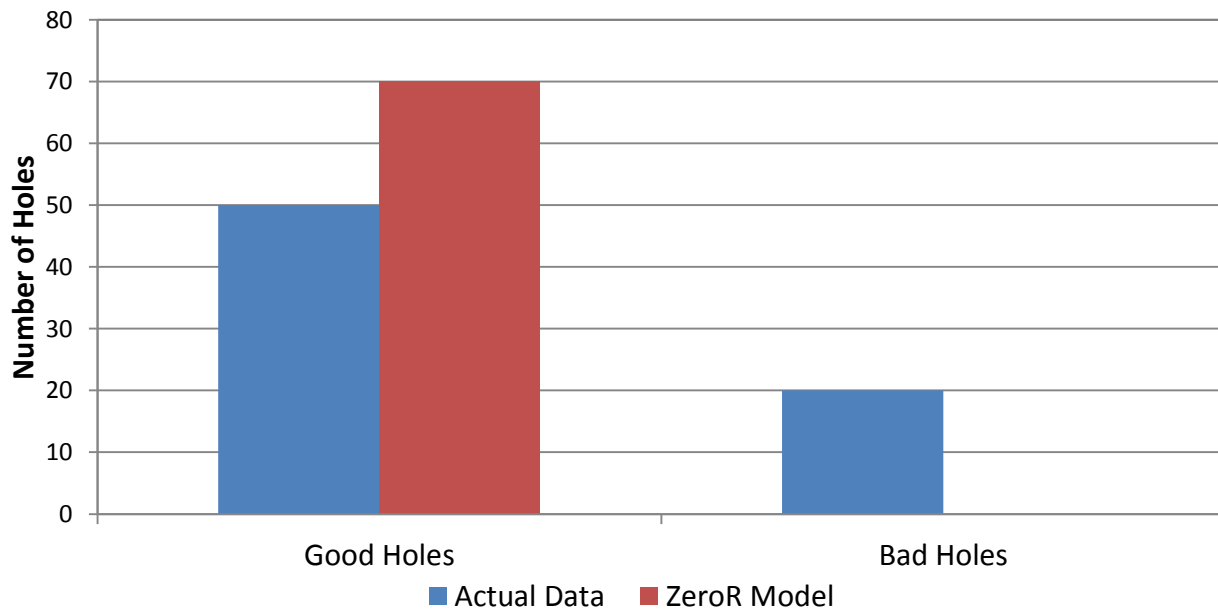


**Figure 13: Graphical representation of the Zero R classifier for generated data**

The confusion matrix is a good way to visualize the output of this ZeroR model as the entire second column is zeros – a bad hole was never predicted.

$$C_{ZeroR} = \begin{bmatrix} \# \text{Good Holes} & 0 \\ \# \text{Bad Holes} & 0 \end{bmatrix}$$

The confusion matrix output of this classifier is a fast way to find the number of good and number of bad holes used in the testing set. For the drilling process, the algorithm also allows for a simple calculation percentage of holes correctly classified by chance.

$$\text{Holes Correctly Classified By Chance} = \frac{C_{ZeroR}(1,1)}{C_{ZeroR}(1,1) + C_{ZeroR}(2,1)} * 100\%$$

Graphically, this percentage can be seen in Figure 13 as the percentage of actual good holes to all holes classified as good by the Zero R model (equal to the total number of holes drilled). As there are significantly more good holes than bad holes (around 96% of holes drilled were good – did not have any tool breakage), the percentage calculated from the Zero R output provides a good comparison point for all other classifiers.

### 6.1.2. Linear Classification Tree

Perhaps the simplest classification algorithm is the linear classification tree. This algorithm uses a decision tree generated based on all model features to classify each hole, Figure 14. Each decision compares the value of a feature to a threshold to determine which branch of the decision tree to travel down. The benefits of using a classification tree are the fast training and response times paired with low memory usage. However, linear classification trees can be prone to over fitting a model to specific data and don't support online learning.

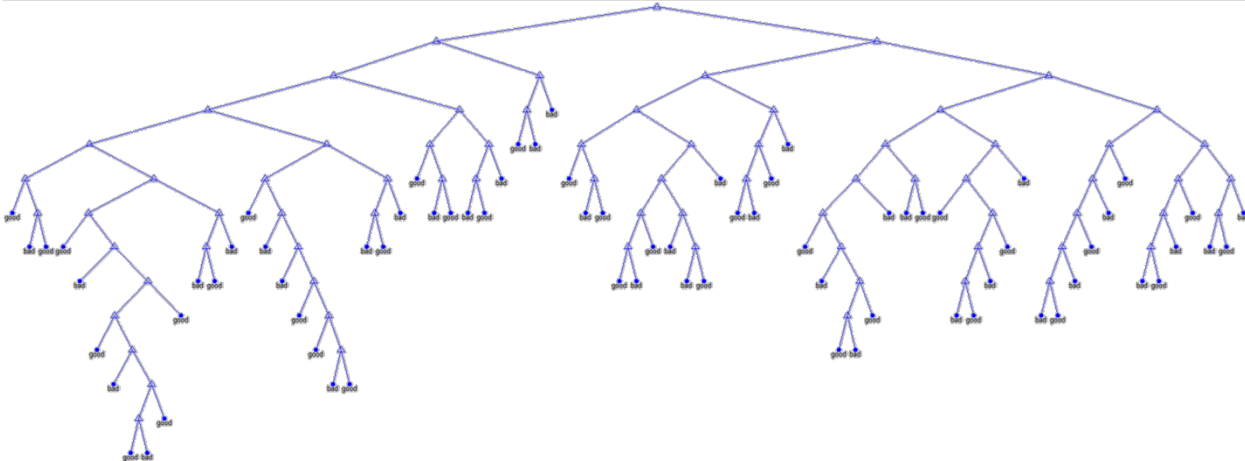


**Figure 14: Classification tree generated from artificial data**

### 6.1.3. Naïve Bayes Classifier

Naïve Bayes (NB) classifiers are simple classifier that uses Bayesian statistics to determine which class a given point belongs to. This classifier works by calculating the centroid of each class using training data and then determining which centroid each test data point is closer to. Theoretically, all features used in a NB classifier must be completely independent of each other (not correlated to any other features). However, in practice a NB classifier can still get useful results even if some of the features are correlated. One of the shortcomings of the NB classifier is its inability to learn interactions between features. Figure 15 shows a NB classifier applied to artificially generated data of good holes (0) and bad holes (1). Note the distances from the centroid of each data set are marked for classifying future points.

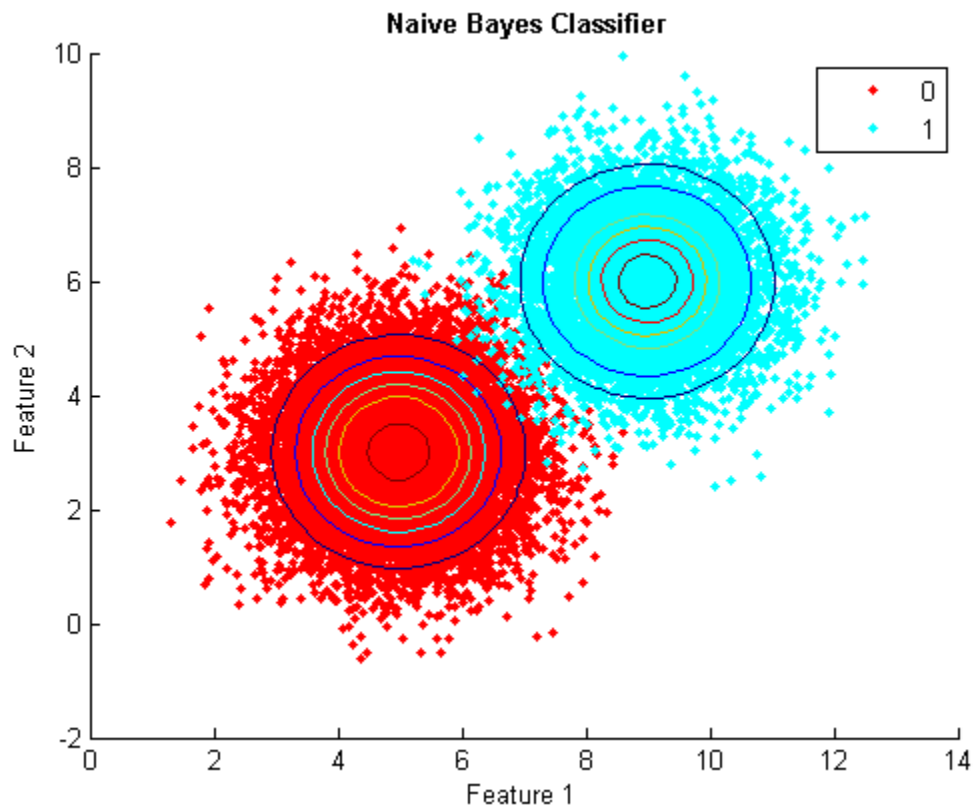


**Figure 15: Two-dimensional naive Bayes classifier generated from artificial data**

### 6.1.4. Linear Discriminant Analysis Classifier

While similar to naïve Bayes classifiers, linear discriminant analysis (LDA) classifiers use a hyperplane to split the data into classes. Similar assumptions are needed for LDA as were used in NB classifiers in addition to the assumption of homoscedasticity. Instead of using Bayesian statistics, LDA uses curve fitting methods split the data set. Figure 16 shows the 2-D artificially generated data split by a hyperplane (in this case a line).

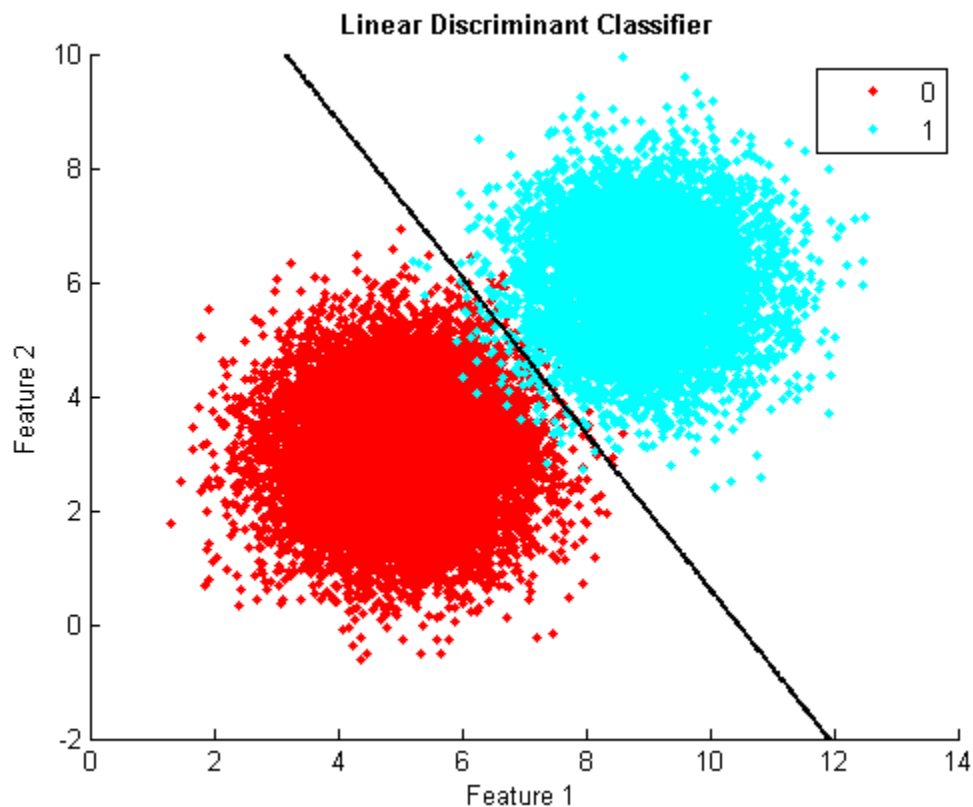


**Figure 16: Two-dimensional linear discriminant classifier generated from artificial data**

### 6.1.5. Support Vector Machine and K-Nearest Neighbor Classifiers

While both support vector machine (SVM) and K-nearest neighbor (KNN) classifiers can be useful classifiers, they were not expected to function well with the collected data. Both of these models can be very accurate, but are very memory intensive when calculating. As there are a very limited number of bad training points, the high accuracy of both SVM and KNN classifiers will likely over fit the data. These models were included in the analysis although they were not

expected to excel with the given data. As such, no time was spend tuning these algorithms and default values were used for parameters such as the number of neighbors in the KNN analysis and the kernel in the SVM model.

## 6.2. Classifier Development

### 6.2.1. Test Classifier Functionality

To ensure that the classifier algorithms were functioning properly they were tested on known, generated data - the same data shown in Figure 15 and Figure 16. This Gaussian artificially generated data met all requirements of the classifiers to work properly. All classifiers tested on the generated data yielded very similar results, as expected, shown below in Figure 17. As the generated data was designed to be neutral, to not favour a certain type of classifier, these results indicate that all classifier models are working properly and that discrepancies seen in the drill data should not be attributed to faulty classifier algorithms.

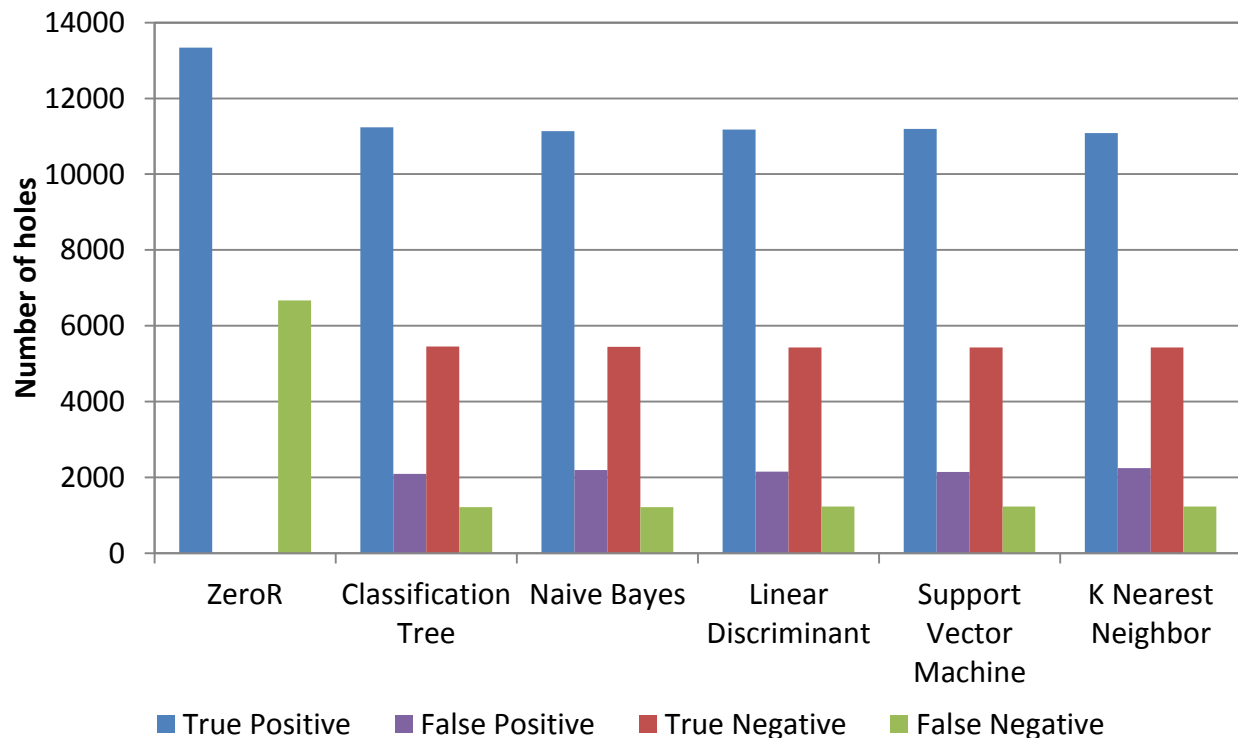


**Figure 17: Results from testing classifiers on artificially generated data**

### 6.2.2. Validate Features

In order to get meaningful results from each classifier the features used must contain some information about the tool breakage state.

Both of the NB and LDA classifiers require all features used to be independent of each other. To test this assumption of independence the Pearson correlations between all 30 of the features tested were calculated. As can be seen in Figure 18, only a few variables have Pearson correlations above 0.9 and most correlations are significantly lower than that. While these few high Pearson correlations are not theoretically ideal for the models, removing the highly correlated features and re-running the analysis yields very similar results on all classifiers. These results imply that the few highly correlated features in the data do not alter the results of the classifier models and they will be left in for the rest of the analysis.

Note that, in general, the correlation between two arbitrary features is not commutative. That is, the correlation of feature X to feature Y is equal to correlation of feature Y to feature X. As such, Figure 18 only shows the correlation between each variable pair once to minimize the number of data points displayed.



From observation of Figure 18 and Figure 19 (a plot of feature values for a run of holes), the most correlated features are:

- AESRmean and AESRrms
- AESFrms and AESFstd
- Fmean and Frms
- Tmin and Tmax and Tmean
- AEWRmean and AEWRrms

Some of these correlations have reasonable physical explanations, i.e. why the RMS and mean values are similar for a given signal. Other correlations, such as the mean of a signal being correlated with the standard deviation, lack a simple physical explanation and may just be by chance. It's also worth noting that all highly correlated features come from the same signal. In other words, features that are calculated from different signals are not highly correlated with each other. This suggests that the signals are independent of each other.

Although some of these features are highly correlated, and therefore not independent, removing these features has a minimal impact on the classifiers output. Removing one of each of the highly correlated pairs of data shows only minor changes (decreases) in classifier output. These small changes (up to a decrease of 1% in classifier accuracy) show how robust the classifier models are against correlated features and also show that the small amount of uncorrelated data contained by the removed features is useful for improving classifier accuracy.

Also from Figure 19 it's apparent that there is no long-term overall trend in values of AEW collected. Holes that were drilled at the beginning of run 05 were significantly further away from the AEW sensor than those drilled at the end of the run. Run 05 was the shortest continuous run collected (124 usable holes) and consists of hole data from the top rows (last drilled) of the second workpiece. The relatively constant values of AEW for all holes backs up the theory that, for workpieces of this size and geometry, attenuation of AE signals on the workpiece has no significant impact on the measured value provided there are no holes or surface imperfections between the drilling location and the sensor.

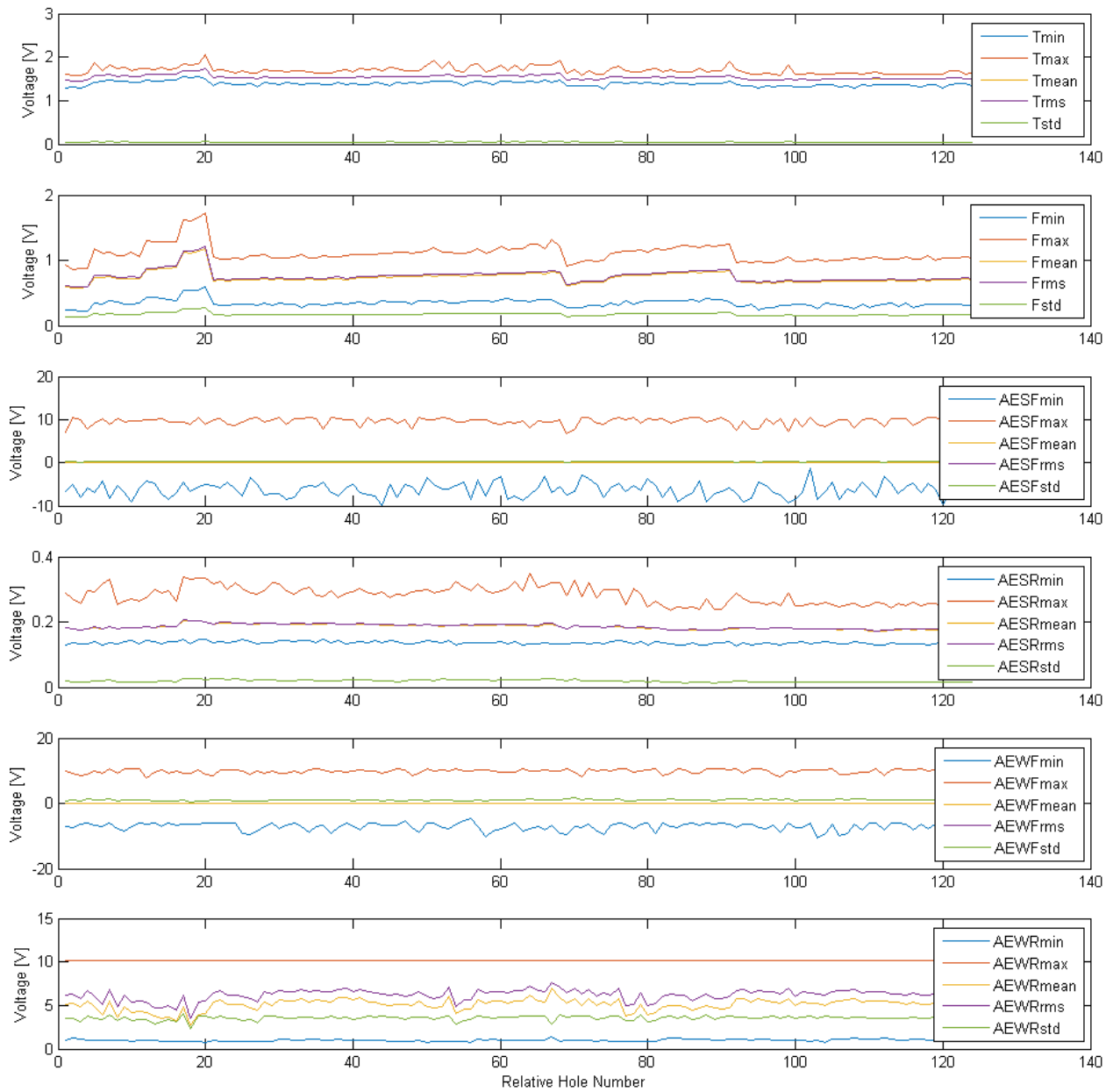


**Figure 19: All features plotted for run 05**

### 6.2.3. Cross Validation

To ensure that all classifiers were given an equal chance at succeeding, a 5 fold cross validation was conducted for each classifier. The cross validation was implemented by splitting the hole data into 5 groups with approximately the same number of failures in each group. The groups were split by the date the data was gathered. Once the 5 groups were chosen, the classifiers were run for every combination of training and testing groups selected from the 5 groups. There were a total of 30 different combinations of training and testing groups run for the cross validation and the results from all 30 trials were averaged for each classifier used. This method of selecting training and testing groups helped ensure that all classifier were treated fairly and the selection of training and testing data didn't favour a certain type of classifier.

After averaging all of the cross validated outputs it was found that there were 1004 *cross validated holes*. Each *cross validated hole* does not have represent a physical hole drilled, instead each represents an average of results from the 30 different testing and training combinations used in the cross validation. Similarly, *cross validated failures* do not represent actual failed holes and as such can have non-integer values.

## 7. Results, Discussion, and Limitations

### 7.1. Results and Discussion

The overall, cross-validated results of the classifier outputs are shown in Figure 20. The figure shows both the percentage of correctly classified holes (good and bad) as well as the percentage of failures detected by each of the classifiers. These two parameters were calculated 3 times for each classifier. The percentages were calculated by running the classifier looking at only outer insert failures, and then only inner insert failures. The third time the two percentages were calculated used a combination of both the outer and inner insert failures (i.e. the outer insert failed or the inner insert failed). Looking at these two percentage parameters for the 3 different cases provides a good starting point for analyzing the best classifier for this given data set.

Using the Zero R classifier as a baseline, it can be seen that the support vector machine (SVM) classifier is unable to correctly classify any bad holes as it performs identical to the Zero R model. This lack of classification power is likely do to the fact that SVM classifiers are low bias/high variance classifiers – which do not work well with small training sets (there were only 35 cross validated bad holes in this data set). K-nearest neighbor (KNN) classifiers are also in the low bias/high variance type of classifiers. For the drilling data collected KNN classifiers were able to correctly classify up to 2.7% of the failures (0.93 cross validated failures detected out of 35). As training sets get larger, both of these classifiers, SVM and KNN, could start to outperform the high bias/low variance classifiers, but with the limited amount of experimental bad holes, both of these classifiers are not useful.

Both the classification tree (CT) and the linear discriminant analysis (LDA) classifiers have very similar results. Both are able to classify around 19% of failures correctly and have the total number of correctly classified holes above 90%; however, the overall classification rate for both of these models is still lower than that of the Zero R model. When looking at combined insert failure, both of these models have a higher combined detection rate than the sum of the inner and outer detection rates. This detection rate relationship between the individual and combined inserts suggests that both of these models are able to pick out features common to both inner and outer insert failure. An intuitive example of this phenomenon would be average torque:

If either the inner or outer insert fails, the mean torque is expected to increase. After collecting the data, looking at an increased value of mean torque for a given hole would suggest that there was an insert failure. However, it would be more difficult to determine which insert failed as torque was expected to increase with the failure of either insert.

The ability of both the CT and LDA models to have increased classification rates for combined inserts suggests that they would be good models to use, perhaps with different, more informative features.

Out of all the classifier models tested, the naïve Bayes (NB) model was able to correctly identify the most failures with a failure classification rate of 45.7%. This high failure classification rate is likely due to the fact that NB models tend to outperform other classifiers when training data is limited. However, even with a very high failure detection rate, the NB model was only capable of an overall classification rate of about 75%. This discrepancy between high failure detection rate and low overall classification rate is due to a large number of false positives, as can be seen in Figure 21. Also, it's interesting to note that the sum of the inner and outer classifications rates exceeds the combined insert classification rate for the NB model by a value of 0.5%. This small difference is interesting and unexpected and could be attributed to the inability of NB classifiers to pick up on interactions between features. The difference could be due to rounding errors in the cross validation as the difference in classification rates translates to only 0.27 cross validated holes out of the total 35 cross validated bad holes.

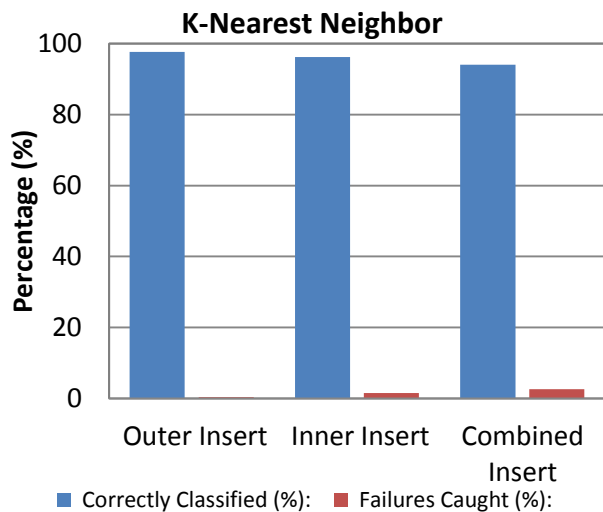
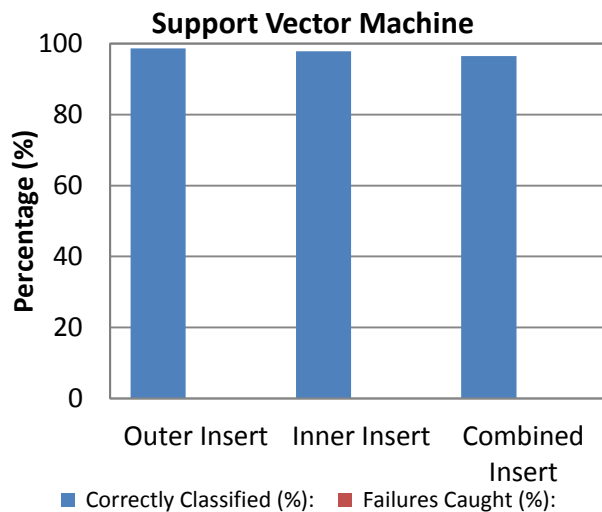
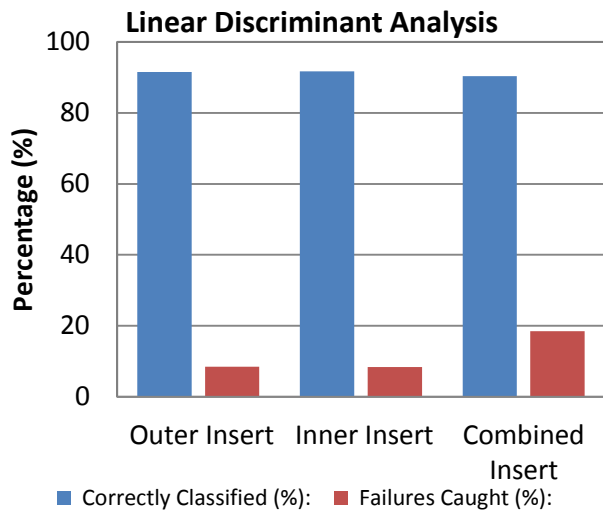
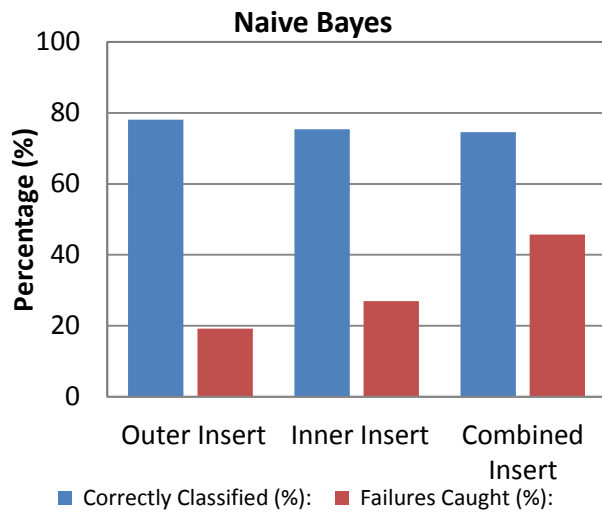
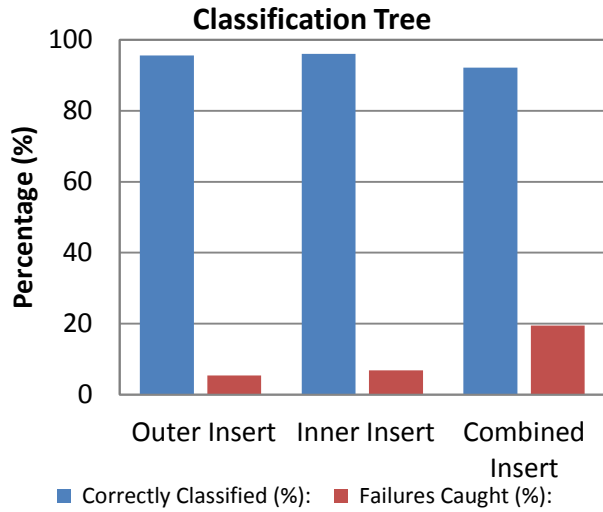
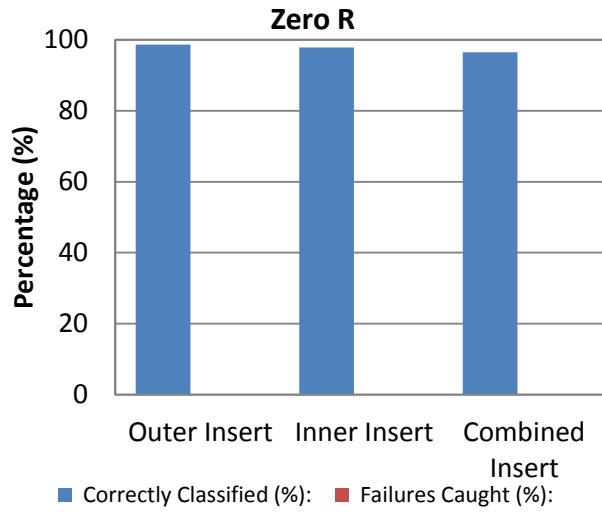


**Figure 20: Cross validated classifier results**

While the NB classifier is the best choice for overall failure detection, it may not be the best suited classifier for the drilling operation. The NB classifier suffers from a large amount of false positives (holes identified as bad that are actually good) when compared to CT and LDA models. The amount of false positives found in these top three models is shown graphically in Figure 21. It can be seen that the amount of false positives for CT and LDA models is on a similar order of magnitude to the amount of true negatives for each case whereas the amount of false positives logged by the NB classifier is a full order of magnitude higher than the amount of failures in the data.

From an operational point of view, increased failure classification rates are worth the tradeoff of increased false positives to a point. However, when false positives are over an order of magnitude higher than the number of failures the usefulness of the model as a means of detecting tool breakage is severely diminished. In the specific case of this research, 236 false positives out of 1004 holes means that 23% of the time the drill will stop when there is no failure – requiring an operator input. Operator input every 5 holes means that a drill running this NB classifier to detect failures will require an operator to do more work than they currently do – resulting in no cost or time savings.

Both the relatively low number of false positives found by the CT and LDA methods and the fact that the combined detection of insert failures is better than the sum of individual detection leads to the conclusion that these types of models are better suited for the drilling application. However, the low failure classification rate implies that the features used in these models do not contain enough information about tool state to work at their full potential.

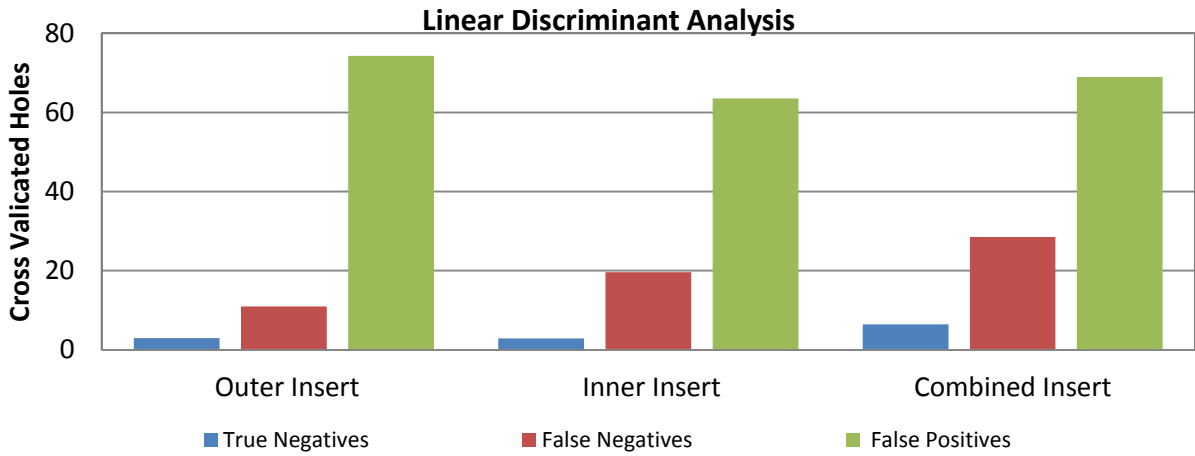
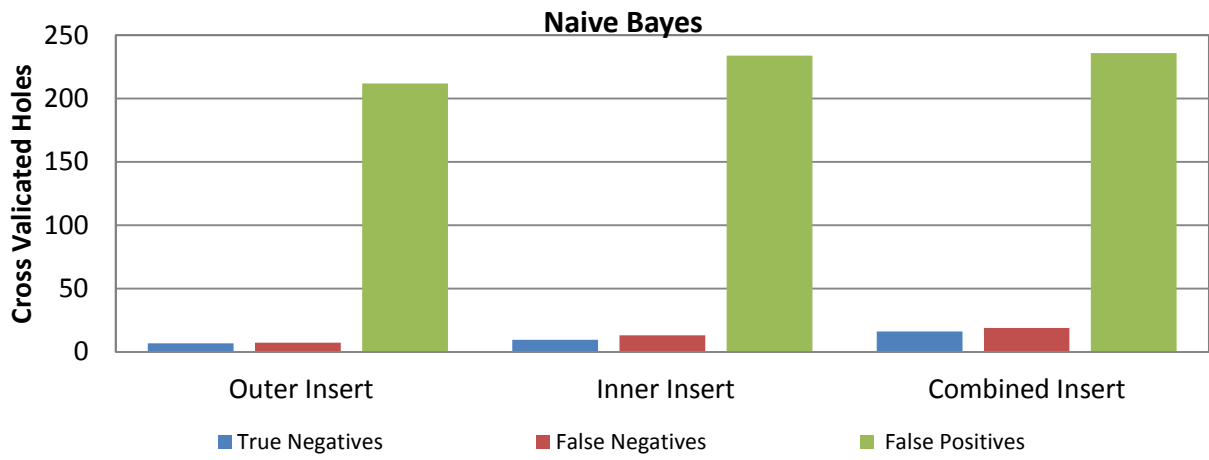
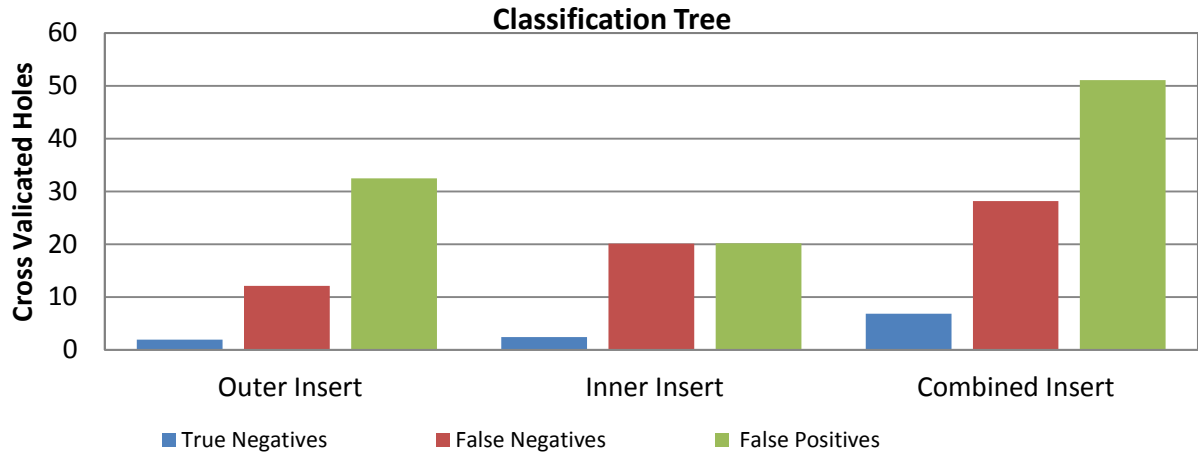


**Figure 21: Confusion matrix outputs for top three classifiers**

In order to determine the usefulness of each of the 30 features, each feature was analyzed to determine the spread of good (denoted in code and figures as 0) to bad holes (denoted in code and figures as 1). The numeric values assigned to all the features can be found in Table 7 and a plot showing the spread of all holes for each feature can be found in Figure 24.

It is difficult to determine which features contain the most information and which, if any, interactions could be useful. A Bayesian method of analysis suggests that the feature with the maximum value of the ratio between the distance between the centroid of good holes and the centroid of bad holes to the sum of the variance of both good and bad holes is the feature that contains the most information. In other words

$$\text{Maximize } \rightarrow \frac{\text{Difference between centroid of good and bad}}{\text{sum of variance of good and bad}}.$$

The features with the largest value of this ratio are the features that have two distinct groups of good and bad holes. It was found that features 21 (AEWFmin) and 5 (Tstd) had the highest values of this ratio and therefore were the most useful – specifically to the NB model. It was also found that features 28 (AEWRmean) and 17 (AESRmax) had the lowest value of this ratio and therefore were the least useful for the NB classifier.

This difference in centroid differences can be seen graphically in Figure 22 and Figure 23. The worst two features plotted against each other in figure Figure 23 have near identical centroids – making it impossible to choose which class (good or bad) a given testing data point belongs to. Figure 22, on the other hand has two distinct centroids making it slightly easier to correctly classify test points.

While looking at this ratio only directly relates to the NB model, it gives a good starting point for the analysis of the usefulness of features. This method does not take into account scenarios where a particular feature identifies good holes at a median value and bad holes at extremes and other methods should be examined to determine feature usefulness.

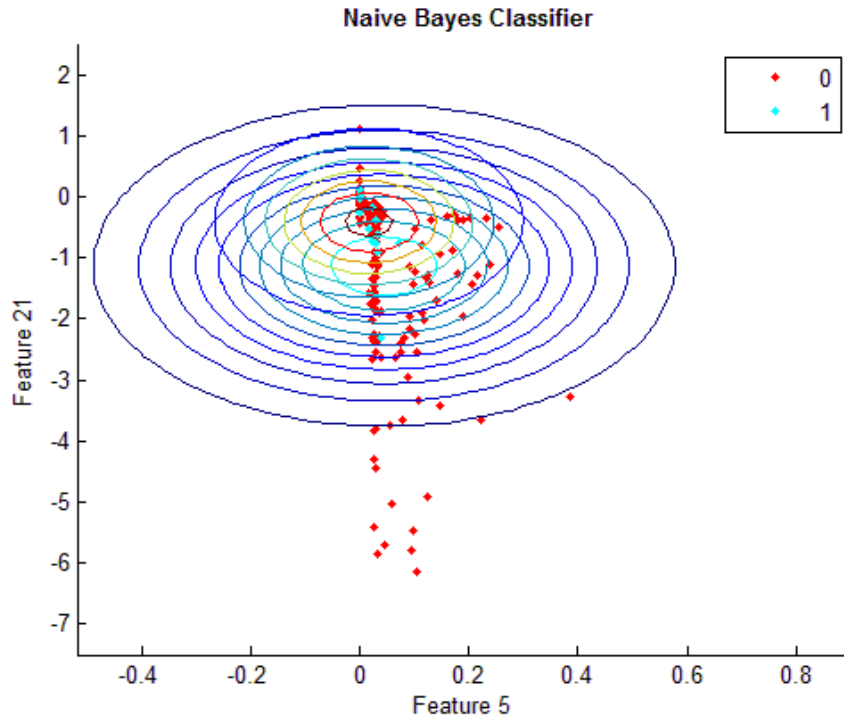


Figure 22: Plot of good and bad holes as feature 21 versus feature 5

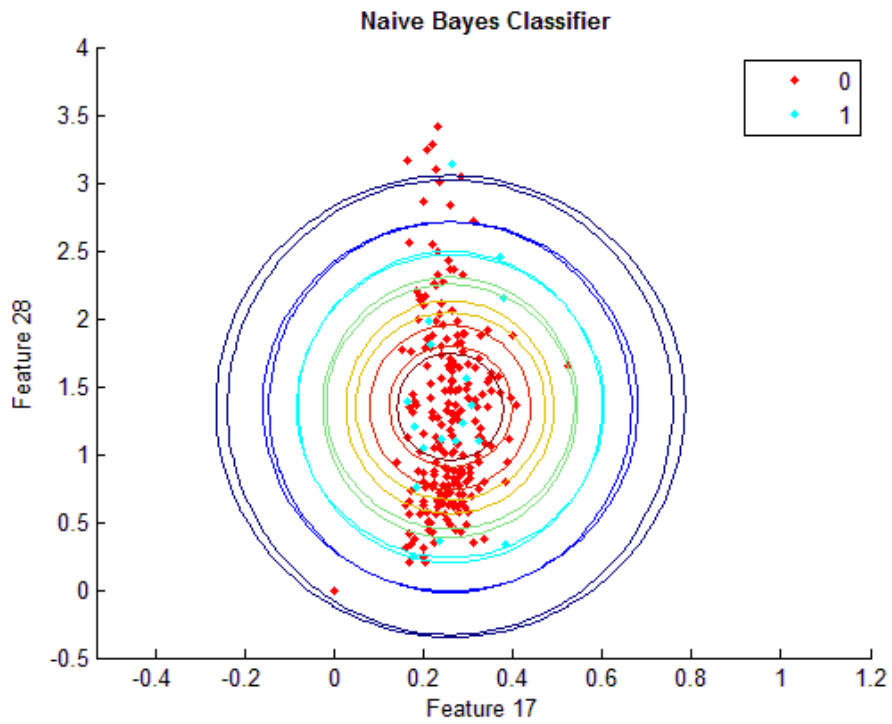


Figure 23: Plot of good and bad holes as feature 28 versus feature 17

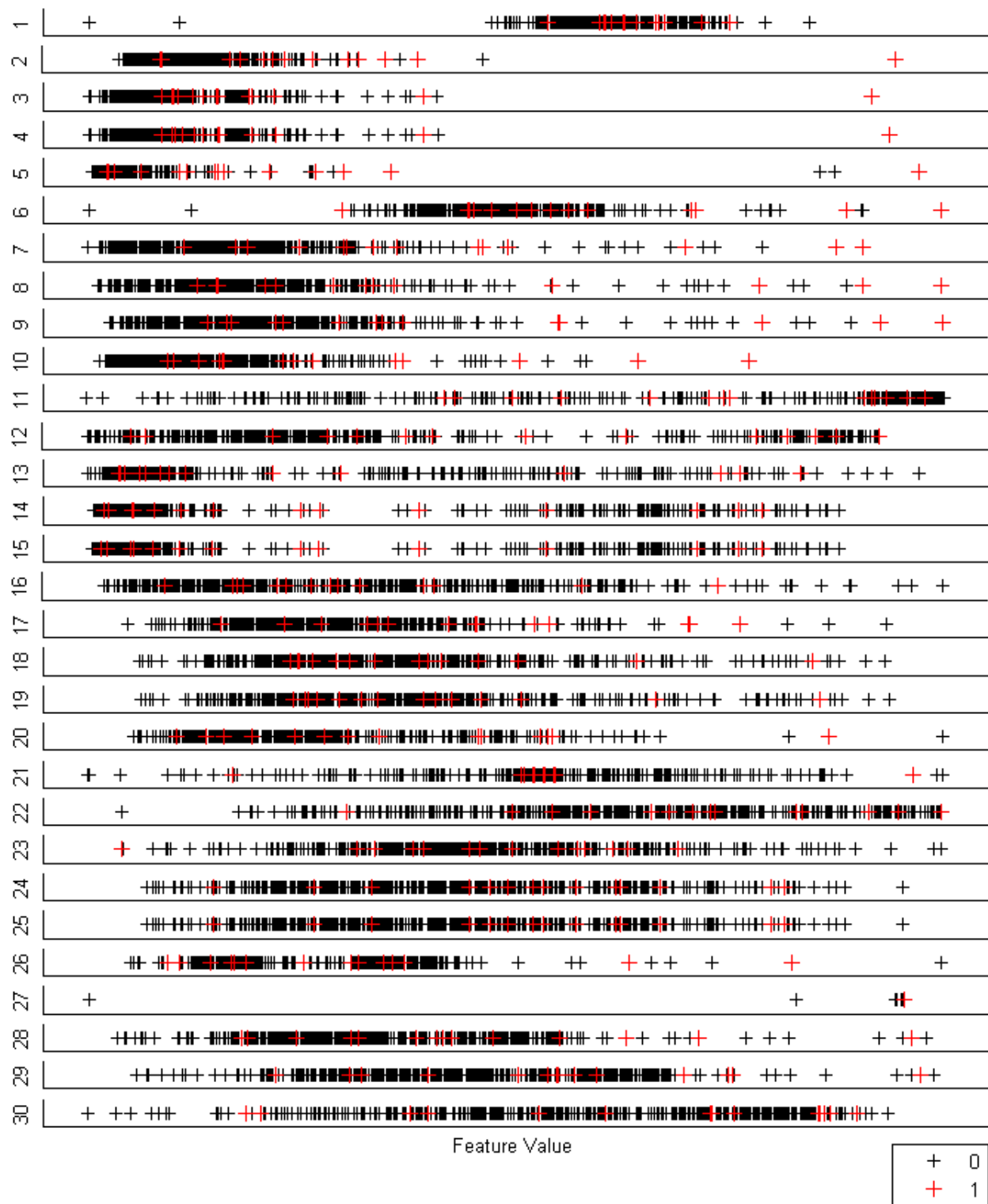


Figure 24: Scatter of all features (by number)

## 7.2. Limitations

One of the limitations and a possible source of error of the data collection process was the fact that holes were drilled in sets of 1-7 holes. This grouping of holes was done to save time on the machine as stopping the drill, checking the inserts, and restarting the drill can take up to 2 minutes and over 2000 holes were drilled. Most of the time when an insert chipped, the operator was able to notice it (by observing the torque, force, sound, and material chips produced) and stop the drill after that hole was complete. However, there were some cases where the insert was inspected after a group of holes was drilled and a chip was found. In these cases, the failure was assigned to the last hole of the group – if it was assigned after inspection of the data it would contain operator or researcher bias. This method of assigning failures may not be perfectly accurate and may skew the results of all classifiers slightly. A possible alternative to this method is to simply discard the data from the group of holes. This alternative was not chosen due to the already low number of bad holes in the data set.

Another limitation of this research is the inability of the model to instantly detect a failure. As time domain features are calculated at the end of a section of the hole, no failure can be detected until after the failed drill has been used to drill part of another hole. While this method can prevent multiple holes worth of damage, it is unable to prevent damage caused to the drill body when using a chipped insert. A method is needed that can instantly detect when a tool is chipped and stop the drill immediately. However, such a method would likely be very susceptible to random environmental noise and be difficult to tune properly.

Analysis was also limited due to the small overall number of failures in the data set. During the 5 fold cross validation, each data set had about 20% of the bad holes (around 15 bad holes in each data subset). As the classifiers were run with 30 features, the cross validated results could have suffered from over fitting as the number of features used was higher than the number of training points in each of the subsets used for cross validation. Analysis, such as principal component analysis, could be done on the features used here as well as new features to select the best features or to create new compound features to remove this source of error from the models.

## 8. Conclusions and Future Work

### 8.1. Conclusions

The main objective of this research project was to develop a system capable of detecting tool breakage and preventing catastrophic failure in large diameter indexable insert drills. To achieve this objective, AE sensors were mounted to both the spindle and workpiece to help collect more information about the condition of the tool than could be collected by the existing torque and force sensors alone. After the sensors were commissioned and installed, a complete data set was collected for drilling 2251 holes. Analysis showed that these AE sensors were successful in collecting useful information and the features from the information helped to increase the classification rate of bad holes in the data. It was suggested that the time domain features extracted from the torque, force, and AE signals be complemented with others features to improve the classification rate.

A number of classifier algorithms were tested using the collected data to find the one best suited to the data set. It was found that CT and LDA models provided the most accurate overall classification rate but the NB model was able to correctly classify the most failures. The cost of the increased failure detection of the NB model was a large number of false positives – an order of magnitude more than was seen in the CT and LDA models. This large number of false detections by the NB model suggests that the CT and LDA models are better suited for detecting failures (perhaps because they can more easily detect interactions between features) given features containing more information about tool condition. Both the SVM and KNN models were found to not be suitable for use with the small data set as they tend to over fit without a large data set but not in depth analysis was done to tune either of these models. If features for enough bad holes were collected, the KNN or SMV models would have a much better chance of providing useful results.

## **8.2. Future Work**

### **8.2.1. Future work on the data analysis**

Future work in the area of tool breakage detection in large diameter indexable insert drills should focus on finding and collecting features that contain more information about tool breakage than the time domain features used. It is possible that frequency domain and time-frequency domain features such as power spectrum densities and wavelets could contain information on tool condition and these features should be tested. Also, features calculated from other portions of the drilling cycle could prove useful. Specifically, features calculated from the beginning and end of each hole could contain more information on tool breakage as it is suspected that entry and exit from the workpiece is the primary cause of tool chipping. Once these features have been found, analysis, such as principle component analysis, should be run to identify the best features or to develop compound features to be used with the new models.

While both CT and LDA classifiers look promising given more informative features, different classifiers could be tested. Specifically, combining two or more classifiers using ensemble methods could increase the failure detection rate while having a minimal effect on the number of false positives generated.

Another potential way to improve the performance of a classifier is to implement a costing or weighting system. With a system such as this, more value could be placed on failures leading to a higher detection rate at the cost of more false positives. These methods could potentially alter less powerful methods like CT or LDA classifiers to perform more like the NB classifier but with potential for less false positives.

### **8.2.2. Future work on experiments**

Future experimental work in this field is suggested to collect more data for more failures. Some of the low bias/high variance classifiers simply did not have enough bad holes to be able to develop a model without over fitting to the training data. Also, splitting the data into groups for cross validation further reduced the number of features tested in each group potentially decreasing the accuracy of some models. By collecting more data, specifically more data for bad holes, using some of the classifiers tested becomes more realistic and accurate. After additional

data collected, methods should be taken to either balance the data set, train with an equal number of good and bad holes, or to compensate for the unbalanced nature of the data.

### **8.2.3. Implementation**

The current algorithm and model use forward predictions and computationally intensive filters. In order to run the model online, new methods for finding holes and dividing holes need to be developed. The current algorithm for finding a hole looks forward in the data to ensure that the torque has increased after a force spike is detected. Also, the  $\alpha$ - $\beta$  filters run as part of the hole division algorithm looks at the data set as a whole and cannot be used in an online system. A possible solution to these issues is tying the overall model in with the G-code running the CNC machine. By tying into the CNC machine, forward predictions are not needed to determine when a hole starts or what portion of the drilling cycle the drill is in.

Additional implementation challenges appear when a drilling parameter or drill size changes. The results of this experiment were compiled from a data set of over 2200 holes – an unacceptably large training set if required for all small changes in the drilling setup. As such, research into scaling factors could prove useful if able to reduce the amount of training data needed when changing drilling parameters.

## References

- [1] R. Griffin, “Tool Condition Monitoring and Replacement for Tubesheet Drilling,” University of Saskatchewan, 2013.
- [2] W. Pease, “An automatic machine tool,” *Sci. Am.*, vol. 187, pp. 101–112, 1952.
- [3] R. L. Kegg, “One-Line Machine and Process Diagnostics,” *CIRP Ann.*, vol. 32, no. 2, pp. 469–473, 1984.
- [4] E. Jantunen, “Indirect multisignal monitoring and diagnosis of drill wear,” 2006.
- [5] A. G. Rehorn, J. Jiang, and P. E. Orban, “State-of-the-art methods and results in tool condition monitoring: a review,” *Int. J. Adv. Manuf. Technol.*, vol. 26, no. 7–8, pp. 693–710, Aug. 2004.
- [6] R. Teti, K. Jemielniak, G. O’Donnell, and D. Dornfeld, “Advanced monitoring of machining operations,” *CIRP Ann. - Manuf. Technol.*, vol. 59, no. 2, pp. 717–739, Jan. 2010.
- [7] S. Cho, S. Binsaeid, and S. Asfour, “Design of multisensor fusion-based tool condition monitoring system in end milling,” *Int. J. Adv. Manuf. Technol.*, vol. 46, no. 5–8, pp. 681–694, May 2009.
- [8] G. Byrne, D. Dornfeld, I. Inasaki, G. Ketteler, W. Konig, and R. Teti, “Tool Condition Monitoring (TCM) - The Status of Research and Industrial Application,” *CIRP Ann.*, vol. 44, no. 2, pp. 541–567, 1995.
- [9] K. Jemielniak, “Commercial Tool Condition Monitoring Systems,” *Int. J. Adv. Manuf. Technol.*, vol. 15, no. 10, pp. 711–721, Sep. 1999.
- [10] E. Jantunen, “A summary of methods applied to tool condition monitoring in drilling,” *Int. J. Mach. Tools Manuf.*, vol. 42, no. 9, pp. 997–1010, Jul. 2002.
- [11] H. M. Ertunc and C. Oysu, “Drill wear monitoring using cutting force signals,” *Mechatronics*, vol. 14, no. 5, pp. 533–548, Jun. 2004.
- [12] K. Jemielniak and P. J. Arrazola, “Application of AE and cutting force signals in tool condition monitoring in micro-milling,” *CIRP J. Manuf. Sci. Technol.*, vol. 1, no. 2, pp. 97–102, Jan. 2008.
- [13] D. E. Dimla, “Sensor signals for tool-wear monitoring in metal cutting operations — a review of methods,” *Int. J. Mach. Tools Manuf.*, vol. 40, pp. 1073–1098, 2000.

- [14] S. C. Lin and C. J. Ting, "Tool wear monitoring in drilling using force signals," *Wear*, vol. 180, pp. 53–60, 1995.
- [15] T. El-Wardany, D. Gao, and M. Elbestawi, "Tool condition monitoring in drilling using vibration signature analysis," *Int. J. Mach. ...*, vol. 36, no. 6, pp. 687–711, 1996.
- [16] I. Abu-Mahfouz, "Drilling wear detection and classification using vibration signals and artificial neural network," *Int. J. Mach. Tools Manuf.*, vol. 43, no. 7, pp. 707–720, May 2003.
- [17] M. Kious, a. Ouahabi, M. Boudraa, R. Serra, and a. Cheknane, "Detection process approach of tool wear in high speed milling," *Measurement*, vol. 43, no. 10, pp. 1439–1446, Dec. 2010.
- [18] S. H. Yeo, L. P. Khoo, and S. S. Neo, "Tool condition monitoring using reflectance of chip surface and neural network," *J. Intell. Manuf.*, vol. 11, pp. 507–514, 2000.
- [19] G. Hermann, "Application of Neural Network Based Sensor Fusion in Drill Monitoring."
- [20] P. Fu and A. D. Hope, "A Hybrid Pattern Recognition Architecture for Cutting Tool Condition Monitoring," no. November, 2008.
- [21] M. Routio and M. Säynätjoki, "Tool wear and failure in the drilling of stainless steel," *J. Mater. Process. Technol.*, vol. 52, no. 1, pp. 35–43, May 1995.
- [22] K. Prasopchaichana and O.-Y. Kwon, "Sensor Fusion by Neural Network and Wavelet Analysis for Drill-Wear Monitoring," *J. Solid Mech. Mater. Eng.*, vol. 4, no. 6, pp. 749–760, 2010.
- [23] K. Patra, "Acoustic Emission based Tool Condition Monitoring System in Drilling," in *Proceedings of the World Congress on Engineering*, 2011, vol. III.
- [24] K. Zhu, Y. S. Wong, and G. S. Hong, "Wavelet analysis of sensor signals for tool condition monitoring: A review and some new results," *Int. J. Mach. Tools Manuf.*, vol. 49, no. 7–8, pp. 537–553, Jun. 2009.
- [25] K. Patra, S. K. Pal, and K. Bhattacharyya, "Artificial neural network based prediction of drill flank wear from motor current signals," *Appl. Soft Comput.*, vol. 7, no. 3, pp. 929–935, Jun. 2007.
- [26] A. L. Quadro and J. R. . Brancoh, "Analysis of the acoustic emission during drilling test," vol. 94–95, pp. 691–695, 1997.
- [27] R. Heinemann and S. Hinduja, "A new strategy for tool condition monitoring of small diameter twist drills in deep-hole drilling," *Int. J. Mach. Tools Manuf.*, vol. 52, no. 1, pp. 69–76, Jan. 2012.

- [28] W. Konig, K. Kutzner, and U. Schehl, "Tool monitoring of small drills with acoustic emission," *Int. J. Mach. Tools Manuf.*, vol. 32, no. 4, pp. 487–493, 1992.
- [29] Sandvik, "Sandvik Coromant," 2014. [Online]. Available: <http://www.sandvik.coromant.com>.
- [30] X. Li and S. K. Tso, "Drill wear monitoring based on current signals," *Wear*, vol. 231, no. 2, pp. 172–178, Jul. 1999.
- [31] Y. T. Oh, W. T. Kwon, and C. N. Chu, "Drilling torque control using spindle motor current and its effect on tool wear," *Int. J. Adv. Manuf. Technol.*, vol. 24, no. 5–6, pp. 327–334, Jul. 2004.
- [32] E. Brinksmeier, "Prediction of Tool Fracture in Drilling," *CIRP Ann.*, vol. 39, no. 1, pp. 97–100, 1990.
- [33] E. Jantunen, H. Jokinen, and R. Milne, "Flexible expert system for automated on-line diagnosis of tool condition," 1996.
- [34] S. S. Panda, D. Chakraborty, and S. K. Pal, "Flank wear prediction in drilling using back propagation neural network and radial basis function network," *Appl. Soft Comput.*, vol. 8, no. 2, pp. 858–871, Mar. 2008.
- [35] M. Kurt, Y. Kaynak, and E. Bagci, "Evaluation of drilled hole quality in Al 2024 alloy," *Int. J. Adv. Manuf. Technol.*, vol. 37, no. 11–12, pp. 1051–1060, May 2007.
- [36] L. A. Franco-Gasca, G. Herrera-Ruiz, R. Peniche-Vera, R. D. J. Romero-Troncoso, and W. Leal-Tafolla, "Sensorless tool failure monitoring system for drilling machines," *Int. J. Mach. Tools Manuf.*, vol. 46, no. 3–4, pp. 381–386, Mar. 2006.
- [37] M. Pirtini and I. Lazoglu, "Forces and hole quality in drilling," *Int. J. Mach. Tools Manuf.*, vol. 45, no. 11, pp. 1271–1281, Sep. 2005.
- [38] S. Dransfeld, "Measurement and Supervision in Automated Production," 2007.
- [39] C. E. Everson and S. Hoessein Cheraghi, "The application of acoustic emission for precision drilling process monitoring," *Int. J. Mach. Tools Manuf.*, vol. 39, no. 3, pp. 371–387, Mar. 1999.
- [40] a. Velayudham, R. Krishnamurthy, and T. Soundarapandian, "Acoustic emission based drill condition monitoring during drilling of glass/phenolic polymeric composite using wavelet packet transform," *Mater. Sci. Eng. A*, vol. 412, no. 1–2, pp. 141–145, Dec. 2005.
- [41] E. P. Serrano and M. A. Fabio, "Application of the Wavelet Transform to Acoustic Emission Signals Processing," vol. 44, no. 5, pp. 1270–1275, 1996.

- [42] I. Tansel, M. Trujillo, a Nedbouyan, C. Velez, W.-Y. Bao, T. . Arkan, and B. Tansel, “Micro-end-milling—III. Wear estimation and tool breakage detection using acoustic emission signals,” *Int. J. Mach. Tools Manuf.*, vol. 38, no. 12, pp. 1449–1466, Dec. 1998.
- [43] X. Li, “Real-time-Detection of the Breakage of Small Diameter Drills with Wavelet Transform,” *Int. J. Adv. Manuf. Technol.*, vol. 14, pp. 539–543, 1998.
- [44] S. Cho, S. Asfour, A. Onar, and N. Kaundinya, “Tool breakage detection using support vector machine learning in a milling process,” *Int. J. Mach. Tools Manuf.*, vol. 45, no. 3, pp. 241–249, Mar. 2005.